High-frequency fluctuations in redox conditions during the latest Permian mass extinction

CrossMark

C. Mettam [a,*], A.L. Zerkle [a], M.W. Claire [a], G. Izon [a,1], C.J. Junium [b], R.J. Twitchett [c]

[a] School of Earth and Environmental Science, and Centre for Exoplanet Science, University of St Andrews, KY16 9AL, UK
[b] Dept. of Earth Science, Syracuse University, NY 13244-1070, USA
[c] Dept. of Earth Science, Natural History Museum, London SW7 5BD, UK

ABSTRACT

New high-resolution geochemical and sedimentological data from Fiskegrav, East Greenland, reveal fluctuations in marine redox conditions associated with the final disappearance of bioturbating organisms during the latest Permian mass extinction (LPME). Sedimentological observations imply a transgressive episode, and associated geochemical evidence for decreasing oxygen availability and the establishment of persistently ferruginous (Fe^{2+}-rich) conditions implies the shoreward migration of oxygen deficient waters. The long-term decline in dissolved oxygen (DO) availability could have been exacerbated by increasing water temperatures, reducing the solubility of oxygen and promoting thermal stratification. Mixing of the water column could have been further inhibited by freshwater influxes that could have generated salinity contrasts that reinforced thermal stratification. Enhanced runoff could also have increased the delivery of nutrients to the marine shelf, stimulating biological oxygen demand (BOD). During the transition to persistently ferruginous conditions we identify intervals of intermittent benthic meiofaunal recolonization, events that we attribute to small transient increases in DO availability. The mechanism controlling these fluctuations remains speculative, but given the possible centennial- to millennial-scale frequency of these changes, we hypothesise that the mid-latitude setting of Fiskegrav during the Late Permian was sensitive to changes in atmospheric circulation patterns, which may have influenced local precipitation and intermittently modulated some of the processes promoting anoxia.

© 2017 The Authors. Published by Elsevier B.V. This is an open access article under the CC BY license (http://creativecommons.org/licenses/by/4.0/).

1. Introduction

The latest Permian mass extinction (~252 Ma) was the greatest biological catastrophe of the Phanerozoic (Benton and Twitchett, 2003; Erwin, 2006; Bottjer et al., 2008; Burgess et al., 2014). The current consensus is that it was a consequence of global warming and associated environmental changes, attributed to an increase in atmospheric carbon dioxide from eruptions of the Siberian Traps Large Igneous Province (e.g. Benton and Twitchett, 2003; Reichow et al., 2009; Algeo et al., 2011; Grasby et al., 2011; Black et al., 2014; Grasby et al., 2017). One of the associated environmental changes that has been invoked as a factor in the marine crisis is ocean stratification and the expansion of anoxic or even euxinic waters during a 'superanoxic' event (Wignall and Twitchett, 1996; Isozaki, 1997; Grice et al., 2005; Riccardi et al., 2006; Shen et al. 2016), or the expansion of oxygen minimum zones (OMZs) onto continental shelves (Stüeken et al. 2015; Clarkson et al., 2016; Lau et al. 2016). Such studies are, however, biased towards low

(tropical) palaeolatitudinal, carbonate-dominated successions of the Palaeo- and Neo-Tethys (Foster and Twitchett, 2014), and condensed sections including the Permian-Triassic boundary global stratotype section and point (GSSP) in Meishan, South China. In comparison, siliciclastic-dominated, stratigraphically expanded successions from higher palaeolatitudes are less-well explored despite some recent work (e.g. Algeo et al., 2012; Schoepfer et al., 2012; Knies et al., 2013; Grasby et al., 2015).

Here we describe findings from a well-preserved, stratigraphically-expanded siliciclastic section that provides an outstanding archive of Late Permian conditions within a marine embayment on the southern margin of the Boreal Ocean at Fiskegrav, East Greenland (Stemmerik et al., 2001; Twitchett et al., 2001; Looy et al., 2001). Existing palaeontological and geochemical data challenge the hypothesis that anoxia had a role in the extinction. Specifically, the transition from bioturbated sediments containing macroscopic shelly fossils to laminated sediments mostly devoid of fossil evidence of marine animals (Stemmerik et al., 2001; Twitchett et al., 2001) appears to predate the onset of anoxia in this section (Fenton et al., 2007; Neilsen et al., 2010).

We have undertaken high-resolution sedimentological and geochemical analyses of strata that record the Late Permian collapse of marine and terrestrial ecosystems (sensu Twitchett et al., 2001; Looy et al.,

---

* Corresponding author.
E-mail address: cwm2@st-andrews.ac.uk (C. Mettam).
[1] Current address: Dept of Earth, Atmospheric & Planetary Sciences, Massachusetts Institute of Technology, Cambridge, MA 02139, USA.

2001), to refine our understanding of physical and chemical conditions during, and in the aftermath of the LPME. Specifically, we have applied Fe speciation to assess changes in water column redox conditions, and sulphur ($\delta^{34}S_{pyr}$), nitrogen ($\delta^{15}N_{bulk}$), and bulk organic carbon isotopes ($\delta^{13}C_{org}$), to examine changes in biogeochemical cycling through this key interval. Our aim is to resolve the stratigraphic relationship between changes in redox conditions and the transition from bioturbated sediments that record the activities of marine benthos, to laminated horizons that are devoid of evidence of macroscopic marine animals or bioturbation (Twitchett et al., 2001). Interrogation of these data will help confirm palaeoenvironmental conditions in marginal Boreal Ocean settings, complementing and expanding upon the body of work available for non-Tethyan domains during this critical period of Earth history.

2. Geological background

2.1. Palaeogeography and biostratigraphy

The Permian-Triassic (P-Tr) strata of Jameson Land, East Greenland (Fig. 1) were deposited within a north-south orientated, fault-controlled embayment (Kreiner-Møller and Stemmerik, 2001; Stemmerik et al., 2001; Wignall and Twitchett, 2002; Müller et al., 2005). Unfortunately the record of shelf conditions within this embayment for the LPME is compromised in many places by erosive submarine channels associated with extensive fan and turbidite deposits (Wignall and Twitchett, 2002; Müller et al., 2005). However, the sedimentary record of the extinction event is preserved at Fiskegrav in a sequence of fine-grained silt- and

Fig. 1. A Fiskegrav locality at 71° 32′ 01.6″ N, 024° 20′ 03.0″ W. Here Late Permian outcrop is shown as grey shading and major faults are shown as ticked lines (Location of Fig. A shown as grey box on inset map B). C Late Permian position of Greenland at ~30°N within Pangea (adapted from Stemmerik et al., 2001).

mud-stones, reflecting deposition in the deepest parts of a sub-basin, but probably at depths of <100 m (Looy et al., 2001; Twitchett et al., 2001; Wignall and Twitchett, 2002; Seidler et al., 2004).

At Fiskegrav, lithologies become slightly finer up section, consistent with a local marine transgression as previously documented for the LPME (Surlyk, 1990; Stemmerik et al., 1993; Kreiner-Møller and Stemmerik, 2001; Haq and Schutter, 2008). Macroscopic shelly fossils (ammonoids, corals, brachiopods) are present lower in the section, but begin to disappear several metres below the top of the Schuchert Dal Fm (Twitchett et al., 2001). The stratigraphically highest Permian brachiopod recorded in the field occurred 1.8 m below the formational contact (Fig. 2). Above this horizon, a limited benthic microfauna of agglutinated foraminifera persist through the section, and fish such as *Bobasatrania* are present in concretions from the base of the Wordie Creek Fm (Stemmerik et al., 2001; Twitchett et al., 2001). Rare small (<1 mm) bivalves and gastropods have been reported from several metres above the base of the Wordie Creek Fm, but the first macroinvertebrate (the bivalve *Claraia*) does not appear until some 14 m above the base of the Wordie Creek Fm (Twitchett et al., 2001). The key portion of the section at Fiskegrav (Fig. 2) is 250 cm thick and contains the contact between the uppermost Schuchert Dal Formation (Fm) and the overlying Wordie Creek Fm and records the cessation of bioturbation (Twitchett et al., 2001).

2.2. The position of the latest Permian mass extinction horizon and Permian-Triassic Boundary at Fiskegrav

Twitchett et al. (2001) and Looy et al. (2001) were the first to document the ranges of key marine and terrestrial fossil taxa through the Fiskegrav section, in association with low resolution C-isotope data. The low diversity macrofauna of Permian brachiopods, corals and ammonoids disappears gradually during the upper few metres of the Schuchert Dal Fm. Following the disappearance of the last Permian macrofossil, however, the rocks remain bioturbated, indicating persistence of a functioning marine ecosystem. Twitchett et al. (2001) used the final disappearance of this bioturbation, which occurred over a ca. 0.8 m interval at the top of the Schuchert Dal Fm, as evidence for a 'marine ecosystem collapse'. This interval coincides with evidence of significant disruption to marine plankton and terrestrial ecosystems (Looy et al., 2001), and correlates well with similar marine collapses identified from the disappearance of bioturbation in other Boreal Sea locations, such as central Spitsbergen (Nabbefeld et al., 2010).

More recently, the C-isotope record has gained favour as a means of correlating the LPME from the GSSP location in South China to Boreal sites. Excursions towards more negative $\delta^{13}C_{org}$ values are widely reported in the Late Permian Boreal record, with initial declines considered to be coincident with the extinction event horizon followed by a protracted and slower fall towards more negative values (e.g. Grasby and Beauchamp, 2008, 2009; Grasby et al., 2015; Dustira et al., 2013). The low-resolution $\delta^{13}C_{org}$ data of Twitchett et al. (2001) suggested that the initial negative $\delta^{13}C_{org}$ shift at Fiskegrav correlates closely to the disappearance of bioturbation and the onset of marine ecosystem collapse; however our higher-resolution data show that the sharp decline in $\delta^{13}C_{org}$ occurred lower in the Schuchert Dal Fm. The start of this decline coincides with the last occurrence of Permian macroinvertebrates (brachiopods) (Fig. 2), and correlates with palynological evidence for the onset of a terrestrial ecosystem collapse (i.e., the decline and loss of cordaite-pteridosperm woodlands and their replacement with more open, herbaceous vegetation; Looy et al. 2001). If the local LPME horizon at Fiskegrav is defined as the start of the $\delta^{13}C_{org}$ excursion and the last appearance of Permian invertebrate macrofossils, then the LPME occurs in the upper Schuchert Dal Fm, some 1.8 m below the base of the Wordie Creek Fm, and predates final marine ecosystem collapse (Fig. 2).

The Permian-Triassic boundary (PTB) is defined at the first appearance datum of *Hindeodus parvus* in Meishan, South China (Yin et al., 1996). At Fiskegrav, *H. parvus* is first recorded ca. 23.5 m above the
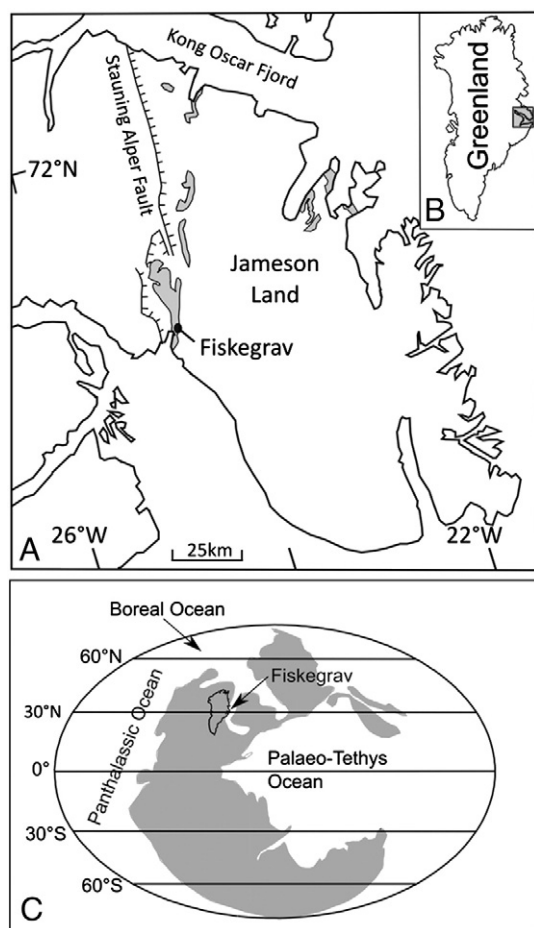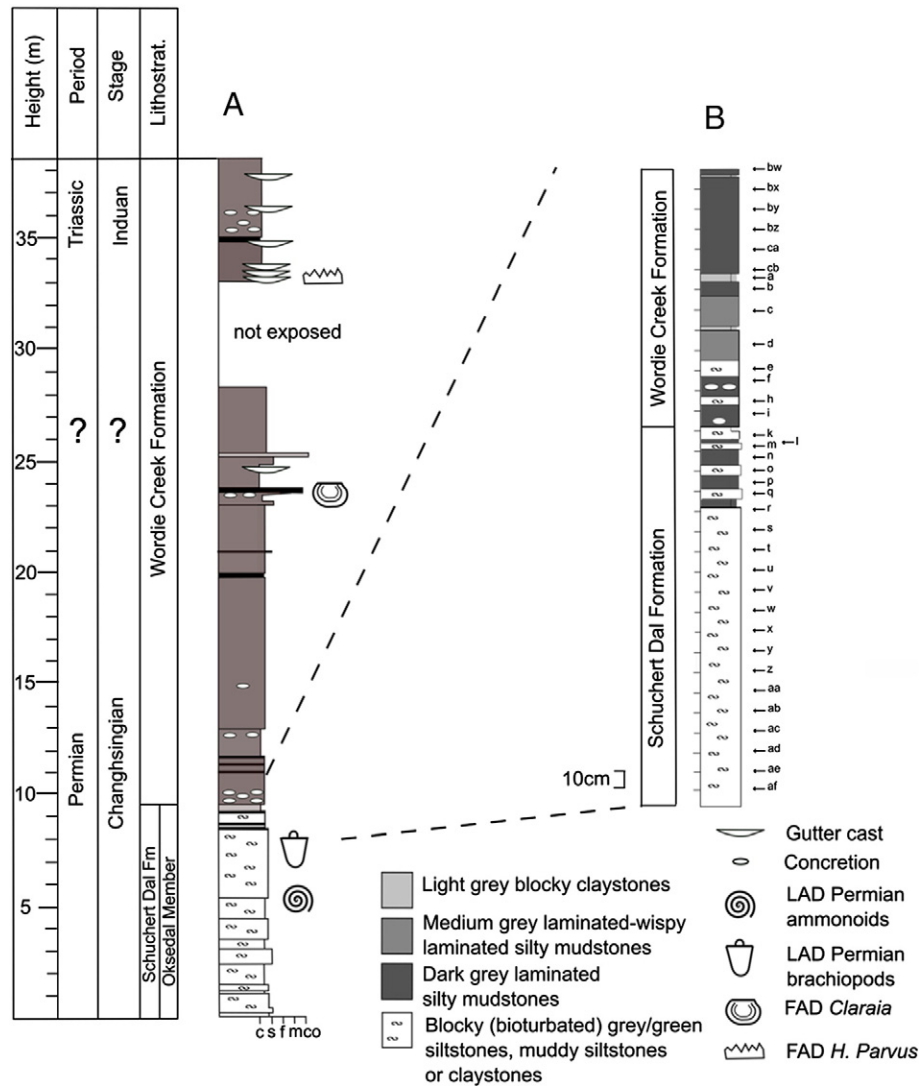
Fig. 2. Sedimentary section at Fiskegrav – **A** Biostratigraphy relevant to the extinction event and the Permian Triassic boundary, adapted from Twitchett et al. (2001). **B** Position of samples in this study. LAD = last appearance datum. FAD = first appearance datum.

base of the Wordie Creek Fm (Twitchett et al., 2001). However, as discussed by Twitchett et al. (2001), it is likely that the actual PTB lies well below this horizon because (a) it is immediately underlain by a ca. 8 m gap in exposure and sampling; and (b) the bivalve *Claraia*, which characterises the Induan in most locations worldwide, occurs ca. 10 m below the first record of *H. parvus* (Fig. 2). For these reasons, Twitchett et al. (2001) suggested that the lowest possible position of the PTB is ca. 10 m above the base of the Wordie Creek Fm. It is possible that future discoveries may reveal Induan-age conodonts or ammonoids even lower within the Wordie Creek Formation, but to date no such fossils have been discovered, even from the concretionary horizons, and so this 10 m datum is assumed to be the lowest possible position of the PTB (Fig. 2). The PTB at Fiskegrav thus occurs between 11.8 and 25.3 m above the local LPME, as defined by the negative $\delta^{13}C_{org}$ shift and the last Permian brachiopod. This stratigraphy would suggest that samples from our study are all Permian in age, and record a period of earth history after the LPME but before the PTB.

2.3. Sedimentation rates

Twitchett et al.'s (2001) original estimates of sedimentation rates at Fiskegrav were derived by correlating Fiskegrav with Meishan, using $\delta^{13}C_{carb}$ and conodont data, and applying the Bowring et al. (1998)

estimate that 700 ($\pm$300) kyr separated the deposition of beds 25 and 28 at Meishan. Using these data, Twitchett et al. (2001) estimated that 1 m of mudstone at Fiskegrav represents on average 20–60 kyr. More recent radiometric age data imply that much less time separates the volcanic ashes of beds 25 and 28 and their equivalents in South China, which in turn suggests much more rapid deposition at Fiskegrav. For example, Shen et al. (2011) suggest that only 180 ($\pm$80) kyr separates beds 25 and 28, with the PTB being dated at 252.17 Ma and the extinction occurring at ca. 252.3 Ma. Using these revised dates, the inferred position of the LPME and the highest and lowest inferred positions of the PTB (Fig. 2; Section 2.2), 1 m of mudstone at Fiskegrav would represent on average between 5 kyr and 11 kyr. More recently still, Burgess et al. (2014) dated bed 25 at 251.941 $\pm$ 0.037 Ma and bed 28 at 251.880 $\pm$ 0.031 Ma, an interval of ca. 60 kyr, with an estimated age for the extinction of 251.950 Ma and for the PTB of 251.902 Ma. These age data imply that 1 m of mudstone at Fiskegrav represents on average between 2 and 4 kyr.

These extremely rapid sedimentation rate estimates are not simply a function of uncertainty surrounding the local position of the PTB at Fiskegrav. Bed 28 at Meishan postdates the *H. parvus* Zone, and at Fiskegrav the *H. parvus* Zone appears to extend to at least the top of the section documented by Twitchett et al. (2001), i.e., at least 30 m above the LPME. These relationships imply sediment accumulation

rates of at least 0.15 m kyr^{-1}, using the Shen et al. (2011) dates, or at around 0.5 m kyr^{-1} using the Burgess et al. (2014) dates. Assuming that recent radiometric ages of Meishan volcanic ashes are correct, 1 m of rock in the studied interval at Fiskegrav represents much <10 kyr and possibly as little as 2 kyr.

3. Methods

3.1. Sample collection and preparation

The studied section at Fiskegrav was logged and sampled by RJT in August 2009. Samples were collected at ~10 cm intervals (Fig. 2) from a shallow trench dug to expose fresh outcrop. Samples were visibly screened for evidence of alteration and approximately 5 g of each sample was homogenised using agate ball mills at the University of St Andrews.

3.2. Fe speciation and major element analyses

Iron speciation measurements were undertaken at the University of St Andrews, following the calibrated sequential extraction procedure developed by Poulton and Canfield (2005) and extended by Clarkson et al. (2014). Following this scheme, redox characteristics of depositional environments can be characterised by the ratios between different pools of iron. The pool of highly reactive iron (Fe$_{HR}$) is defined as the summation of pyrite iron (Fe$_{PY}$) and other Fe species such as carbonate iron (Fe$_{Carb}$), iron oxide (Fe$_{Ox}$) and magnetite iron (Fe$_{Mag}$), which are reactive towards hydrogen sulphide (H$_2$S) and have the potential to produce pyrite in the water column or during early diagenesis (Fe$_{HR}$ = Fe$_{Carb}$ + Fe$_{Ox}$ + Fe$_{Mag}$ + Fe$_{PY}$). Oxic depositional conditions are indicated when the ratio of highly reactive iron to total iron (Fe$_{HR}$/Fe$_T$) ≤ 0.22, whilst a ratio of Fe$_{HR}$/Fe$_T$ ≥ 0.38 indicates unambiguously anoxic depositional settings (Poulton and Canfield, 2011). Anoxic depositional settings can be further subdivided into ferruginous (Fe^{2+}-rich), or euxinic (sulphidic) conditions. Traditionally, unambiguously euxinic depositional conditions have been inferred when the Fe$_{PY}$/Fe$_{HR}$ ratio ≥ 0.8, however recent work indicates a Fe$_{PY}$/Fe$_{HR}$ ratio of ≥0.7 may be indicative of euxinia (Poulton and Canfield, 2011; Poulton et al., 2015). Full descriptions of the chemical extraction protocol and iron concentration measurements performed at St Andrews have been described previously (Izon et al., in press) and are appended in the supplementary information.

Reproducibility of Fe$_{Carb}$, Fe$_{Ox}$ and Fe$_{Mag}$ pools determined by synthetic, matrix matched, 1 ppm Fe standards (n > 5 in each run) was better than 2% (1σ; RSD); whereas, reproducibility of replicate extractions of PACS-2 (n = 5) was better than 5% (1σ; RSD). Experimental triplicates (using sample 09.8.29.bx) for the distillation process demonstrate a 1σ RSD better than 5% for determination of Fe$_{PY}$. Reproducibility of XRF analyses to determine Fe$_T$ was assessed by experimental comparison with Penryhn slate, where a value of 8.95 ± 0.04% (3σ, n = 20) was obtained against a certified value of 8.94%. Other elemental oxides provided comparable reproducibility.

3.3. TOC, TN and stable isotope analyses

Analyses of total organic carbon content (TOC), bulk organic carbon isotope ratios (δ^{13}C$_{org}$) and bulk nitrogen isotope ratios (δ^{15}N$_{bulk}$) were performed on decarbonated rock powders. Decarbonation involved subjecting ca. 0.5 g of homogenised, whole-rock powder to two 24-h, 10% (vol/vol) HCl leaches. Sample residues were then washed until pH neutral using Type 1 ultrapure (18.2 MΩ•cm) water and dried at <40 °C. Carbonate content was then calculated gravimetrically from dry sample residues.

Total organic carbon and total nitrogen (TN) content were determined at the Imaging and Analysis Centre, Natural History Museum, London, with all samples measured in triplicate using an Elementar Vario Microcube elemental analyser. Replicate analyses of the commercial standard 'sandy soil' were statistically indistinguishable from the certified abundance value for carbon of 0.833% ± 0.05 (1σ; n = 8) and of 0.07% ± 0.01 (1σ; n = 5) for nitrogen.

Bulk organic carbon isotope values (δ^{13}C$_{org}$) were measured by analysis of decarbonated rock powders at the University of St Andrews via standard Elemental analyser-isotope-ratio mass spectroscopy (EA-IRMS) techniques. Data accuracy was verified using an internal sucrose standard (n = 5), with precision better than ±0.1‰ (1σ). A subset of δ^{13}C$_{org}$ analyses were performed by Iso-Analytical Laboratories, Cheshire, UK, via standard EA-IRMS methods. Standard IA-R001 provided a mean δ^{13}C$_{org}$ value of −26.42‰ (n = 9), with a standard deviation of 0.05‰ (1σ) against a certified value of −26.43 ± 0.08‰ (1σ). Sulphur isotopes (δ^{34}S$_{pyr}$) analyses were performed on the silver sulphide (Ag$_2$S) precipitated during the CrCl$_2$ (Fe$_{PY}$) distillation by Iso-Analytical Laboratories, Cheshire, UK, using standard EA-IRMS techniques. Data accuracy was assessed using reference materials IA-R061 with reproducibility of ±0.11‰ (1σ; n = 10), and IAEA-SO-5 with reproducibility of ±0.2‰ (1σ; n = 10). Low TN abundances necessitated that nitrogen isotope ratios were determined by nano-EA-IRMS at Syracuse University, USA. Data accuracy was assessed using IAEA N1 (Ammonium Sulphate, (NH$_4$)$_2$ SO$_4$; n = 9). Mean δ^{15}N value for this standard was −0.04‰ and standard deviation was better than 0.27‰ (1σ, n = 9), against a certified value of +0.4 (±0.2‰; 1σ). Detailed procedures are presented in the supplementary information.

All isotopic values are reported in standard delta notation showing per mil deviations from international standards as follows:

$$\delta^a X\ (‰) = \left(\left(^a X/^b X\right)_{sample} / \left(^a X/^b X\right)_{standard} - 1 \right) \times 1000 \qquad (1)$$

Where $^a X/^b X$ is the ratio between the heavier (a) and the lighter isotope (b) of element X. Ratios are reported to relevant standards: δ^{13}C (relative to V-PDB), δ^{15}N (relative to air), and δ^{34}S (relative to V-CDT).

4. Results

4.1. Lithology

Field observations at Fiskegrav reveal a slight fining of grain-size and a transition from bioturbated to laminated mudstones around the contact between the Schuchert Dal and Wordie Creek formations. For the purposes of this study, the studied section has been divided into four broad Intervals based on lithological properties (Figs. 3 and 4). Interval 1 is entirely within the Schuchert Dal Fm, extending from the base of the studied section to 40 cm below the contact with the overlying Wordie Creek Fm. It is bioturbated throughout and composed of blocky, grey/green siltstones and muddy siltstones. Samples from the 50 cm section below Interval 1 were analysed for carbon isotope (δ^{13}C$_{org}$) values only, allowing for chemostratigraphic comparison with other sections. Interval 2 spans from the top of Interval 1 to 35 cm above the formational contact, and is composed of dark-grey, laminated, silty mudstones. Within Interval 2 there are 6 beds of bioturbated, blocky, grey/green muddy siltstones, silty mudstones or claystones, which are each <10 cm thick, and are similar to those described in Interval 1. These bioturbated beds are separated by unbioturbated, laminated horizons. The base of the Wordie Creek Fm is marked by the appearance of small nodules containing fossil fish. Interval 3 is ca. 30 cm thick and is composed of medium-grey, laminated silty mudstones with a thin bed of light-grey blocky claystone at ca. 50 cm above the formational contact. The uppermost Interval 4 consists of ca. 75 cm of dark-grey, laminated-, silty-mudstones, with thin beds of light-grey blocky claystone at 85 cm and 125 cm above the formational contact.
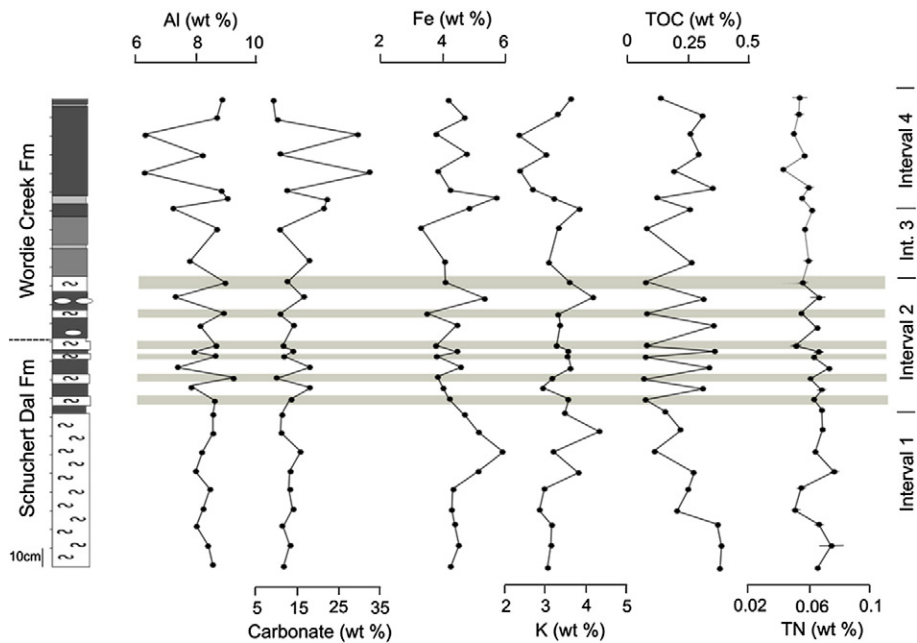
Fig. 3. Bulk chemical measurements. Horizontal shaded bars indicate bioturbated horizons in Interval 2.

4.2. Bulk rock geochemistry

Total organic carbon content through the section is generally low (mean = 0.2 wt%; Fig. 3; Table S3), consistent with results from previous studies (Oberhänsli et al., 1989; Stemmerik et al., 2001; Twitchett et al., 2001). TOC abundance declines through Interval 1, and then values fluctuate within Intervals 2, 3 and 4. The lowest values in the entire section are in Interval 2, but these low wt% TOC are restricted to bioturbated horizons, with higher wt% TOC in laminated horizons. Similar fluctuations in TOC occur in Interval 3 and the lower portion of Interval 4, although these variations do not appear to be related to obvious lithological changes. Mean TN abundances are 0.06 wt% for the whole section, but show a subtle decline up-section (Fig. 3; Table S3). There is variability in TN in Interval 2, with higher TN abundances within laminated Intervals, although this variability is less pronounced than that of TOC. The mean TOC/TN ratio for the whole section is 3.7;
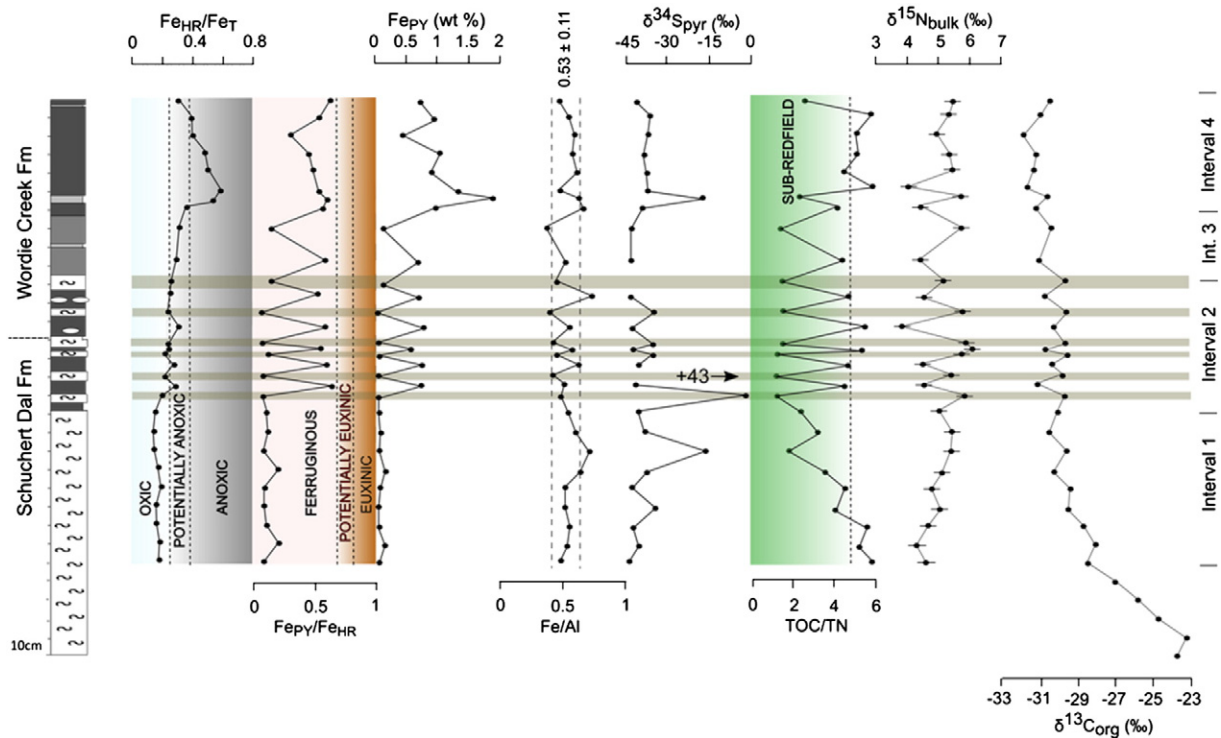

Fig. 4. Fe speciation, TOC/TN and stable isotope data. Horizontal shaded bars indicate bioturbated layers in Interval 2. Fe speciation thresholds are shown by differential shading in plots of Fe_{HR}/Fe_T and Fe_{PY}/Fe_{HR}. Average Fe/Al ratio of 0.53 ± 0.11 (Lyons and Severmann, 2006; Raiswell et al., 2008) is shown by vertical dashed lines in plot of Fe/Al. Redfield ratio for marine organic matter shown by graded shading in plot of TOC/TN (Gao et al., 2012).

it declines through Interval 1 but shows variability in Interval 2, with higher TOC/TN ratios occurring in laminated horizons. Variability in TOC/TN ratios also occurs in Interval 3 but is not linked to lithology (Fig. 4; Table S3).

Mean carbonate content for the section is 14.5 wt% and shows a general increase up-section (Fig. 3; Table S3). In Interval 1, carbonate content is relatively constant, but becomes increasingly variable up section. In Interval 2 this variability is tied to lithology, with laminated horizons having higher carbonate content than bioturbated horizons. Fluctuations in carbonate content continue in Intervals 3 and 4 but are not linked to lithological changes.

Mean Al content is 8.2 wt%, with increasing variability up section (Fig. 3; Table S2). In Interval 2 this variability is related to lithological changes, with higher Al content found in bioturbated horizons. Mean Fe content is 4.4 wt% (Fig. 3; Table S2). Fe abundances rise through Interval 1, before declining in the lower part of Interval 2 where they begin to fluctuate. Notably, Fe concentrations are highest in laminated layers and lowest in bioturbated layers, apart from relatively low values within a laminated horizon 30 cm below the base of the Wordie Creek Fm. Variability in Fe abundance increases in Intervals 3 and 4 despite a lack of lithological variation. Potassium (K^+) content has a mean value of 3.3 wt% (Fig. 3; Table S2). Some variability occurs in Interval 2 but is not coupled to changes in lithology; variability is greater in Intervals 3 and 4, despite their relatively constant lithologies.

4.3. Iron speciation

Fe_{HR}/Fe_T ratios range from 0.15 to 0.59, with a mean value 0.28 (Fig. 4; Table S1). Interval 1 shows Fe_{HR}/Fe_T ratios consistently below 0.22. Although Fe_{HR}/Fe_T ratios increase through Intervals 2 and 3, they do not exceed 0.38 until Interval 4. Variability is recorded in Interval 2, with slightly higher Fe_{HR}/Fe_T ratios in laminated horizons. Similarly, Fe_{PY}/Fe_{HR} ratios display a constant and low background throughout Interval 1; however, in contrast with Fe_{HR}/Fe_T ratios, Fe_{PY}/Fe_{HR} ratios vary considerably in the overlying Intervals. Variability in Fe_{PY}/Fe_{HR} in Interval 2 is driven by fluctuations in Fe_{PY} abundance, with higher Fe_{PY} abundance in laminated beds. Further fluctuations in Fe_{PY}/Fe_{HR} are recorded in Interval 3, which again appear to be influenced primarily by Fe_{PY} abundance variations that occur despite lack of lithological variation. Fe/Al ratios are predominantly within the Fe/Al thresholds for Phanerozoic sediments of 0.53 ± 0.11, as established by Raiswell et al. (2008).

4.4. Stable isotope data

Mean $\delta^{13}C_{org}$ for the whole section is −29.5‰, with a standard deviation of 2.1‰ (1σ) (Fig. 4; Table S3). $\delta^{13}C_{org}$ values decrease up-section, beginning with a rapid fall below Interval 1 followed by a more gradual decline above. As with other geochemical data, the $\delta^{13}C_{org}$ values are variable in Interval 2, with slightly less negative $\delta^{13}C_{org}$ in bioturbated beds. The mean $\delta^{15}N_{bulk}$ value for the whole section is 5.1‰, standard deviation of 0.6‰ (1σ) (Fig. 4; Table S3). In Interval 1, $\delta^{15}N_{bulk}$ values are lower, but record a general trend towards more positive values up-section. In Interval 2, $\delta^{15}N_{bulk}$ values fluctuate considerably, approximating the mean within bioturbated layers, but displaying lower values in laminated horizons. The exception is one $\delta^{15}N_{bulk}$ measurement at ca. 5 cm below the base of the Wordie Creek Fm, where the maximum $\delta^{15}N_{bulk}$ value of 6.1‰ occurs within a laminated horizon. The $\delta^{15}N_{bulk}$ values also vary within Intervals 3 and 4 despite little observed lithological variation, but this variability in $\delta^{15}N_{bulk}$ values becomes less pronounced at the top of the section. Most $\delta^{34}S_{pyr}$ values are close to the mean of 36.5‰, but a few samples, mainly from bioturbated horizons are ^{34}S-enriched, leading to a standard deviation of 9.5‰ (1σ) (Fig. 4; Table S3).

5. Discussion

5.1. Reliability of geochemical data

The geochemical composition of sedimentary rocks, and hence the palaeoenvironmental information they contain, may become modified by post depositional processes associated with diagenesis and metamorphism. To ensure that our geochemical data provide a faithful record of conditions during deposition, a range of standard evaluations were conducted and confirm that our data are robust. Details of these geochemical evaluations are given in the supplementary material.

5.2. Evidence of marine transgression

Trends in lithology and bulk geochemical data are all consistent with a transgression in the Fiskegrav section, with slightly finer material up-section indicating deeper, lower-energy conditions. However, in addition to a shift to lower energy conditions, other factors may control grain size. Slightly coarser-grained bioturbated horizons lower in Interval 1 generally record lower TOC/Al, Fe_{PY}/Al and carbonate/Al ratios, whilst high abundances of TOC, carbonate and Fe_{PY} are generally recorded in laminated horizons (Figs. 3, 4, 6 A, B, C, D and E). These data could indicate a higher detrital input of silicates (e.g. detrital clays/micas) within shallower, more proximal depositional settings within Interval 1, although such a conclusion is not supported by variations in potassium abundances (Fig. 3), which are a further proxy for terrestrial input. In Interval 2 and above, the presence of slightly finer grains within laminated beds is not likely to be the result of minor transgressions or reduced terrestrial inputs. Rather, smaller grain sizes and relatively low aluminium abundances in laminated horizons of Interval 2 and above probably reflect the influence of redox changes (as identified by Fe speciation data; Sections 5.3 and 5.5) leading to the dilution of aluminium abundances. For example, lower oxygen availability in laminated horizons could promote the preservation of organic matter and enhanced microbial sulphate reduction (MSR) could promote higher Fe_{PY} abundances. Another important factor causing low Al abundances in laminated horizons is likely dilution by increased carbonate abundances. Increased carbonate abundance in laminated horizons could reflect authigenic carbonate cements produced in association with anaerobic oxidation of methane coupled to MSR (Hovland et al., 1987; Peckmann et al., 2001). The formation of carbonates by such processes could explain the anomalously low ca. −10‰ $\delta^{13}C_{carb}$ values previously recorded in the lower Wordie Creek Fm (Twitchett et al., 2001). Böttcher (2011) also argued that authigenic manganese–calcium carbonates, with minor incorporation of magnesium and divalent iron, can form during suboxic and anoxic early diagenesis under brackish marine conditions, similar to the conditions which we infer for the deposition of laminated horizons (Section 5.3).

5.3. Palaeoredox evolution

Our Fe speciation data indicate a transition to lower oxygen availability up section, although unambiguously anoxic conditions only became established within Interval 4. This change is consistent with an increasing influence from anoxic waters formed deeper on the shelf, in association with the previously documented marine transgression. Anoxic waters were probably generated on the deeper shelf by high BOD fuelled by the degradation of organic matter beneath a thermally stratified water column (Friedrich et al., 2014). The intensification of oxygen deficiency at Fiskegrav may have been related to several factors. Rapid temperature increases leading to high sea surface temperatures have been proposed for the Late Permian, with oxygen isotope ($\delta^{18}O$) data from conodont apatite indicating a rise from ca. 24 °C to ca. 33 °C between the extinction horizon (bed 25) and the PTB (bed 28) in the Meishan and Shangsi sections in China (Joachimski et al., 2012; Sun

et al., 2012). Temperature rises over the shorter time-span in the higher palaeolatitude section studied at Fiskegrav have not been established, but might also have been significant. These increases in water temperatures could have further reduced the solubility of oxygen in sea water (e.g., Matear and Hirst, 2003), whilst enhancing thermal stratification. Increased fluxes of nutrients due to increased chemical weathering could have been delivered to the shelf (e.g. Algeo et al., 2011) promoting BOD. These fluxes are feasible, as enhanced erosion of terrestrial biomass and other material are consistent with the probable availability of dead plant material associated with reported changes in terrestrial flora (Looy et al., 2001), which could have enhanced weathering and erosion by destabilizing soils.

Further, we speculate that the transport of terrestrial nutrients to the shelf was facilitated by enhanced run-off resulting from changes in precipitation due to a combination of the palaeolatitudinal setting of Fiskegrav and processes associated with rapid global warming. We speculate that when oxic conditions prevailed in the water column during the deposition of Interval 1, the depositional site of Fiskegrav at 30°N during the Late Permian may have been under the influence of the Mid-Latitude Cell, where predominantly offshore winds from the west (Fig. 5A, C) would have been relatively dry after passing over a significant land mass. Alternatively, this site could have been located under the cool descending air and high pressure conditions where the Hadley and Mid-Latitude Cells meet. Rapid global warming (Joachimski et al.,
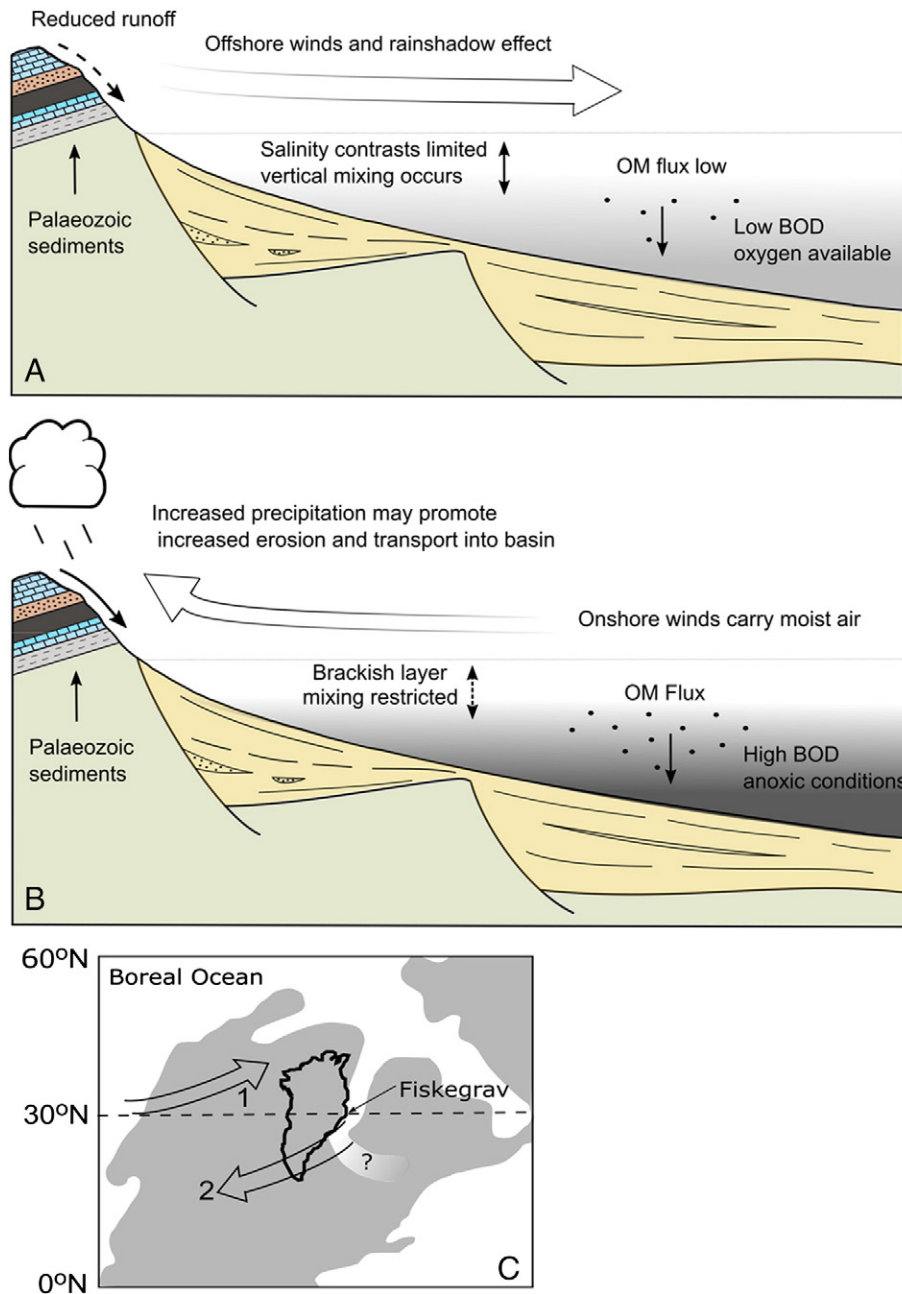

Fig. 5. Hypothesised depositional setting at Fiskegrav. **A** Offshore winds - air is dry restricting precipitation. Runoff and erosion are low. **B** An expansion of the Hadley Cell brings Fiskegrav under the influence of relatively moist on-shore winds. Higher precipitation facilitates erosion and transport of nutrients to shelf. BOD is enhanced expanding oxygen deficient waters. Salinity contrasts reinforce thermal stratification, reducing mixing. **C** Prevailing wind directions in Hadley Cell (from east) and Mid-Latitude cell (from west). Map adapted from Stemmerik et al. (2001), (see Fig. 1C) with grey areas showing emergent land. Question mark and lighter shading show approximate site of Zechstein basin which Stemmerik et al. (2001) show as marine, but may not have been open at this time. Glennie et al. (2003) have suggested that the southern margin of the Boreal Ocean progressively migrated southwards over the Late Permian. The maximum width of the embayment at in the Late Permian was likely ca. 80 km (Stemmerik et al., 2001), although earlier estimates suggest it could have been as wide as 400 km (Doré, 1991).

2012; Song et al., 2014) could have led to the pole-ward expansion of the boundaries of this Hadley Cell (e.g. Lu et al., 2007; Kang and Lu, 2012). This change in circulation patterns could have brought Fiskegrav under the influence of relatively moist onshore winds (Fig. 5B, C), stimulating a relative increase in precipitation and terrestrial runoff during deposition of Intervals 3 and 4. Importantly, this influx of fresh water could have created vertical salinity contrasts, amplifying thermal gradients and further restricting water column mixing.

The intensification of anoxia at Fiskegrav is unlikely to be related to an increase in the upwelling of nutrients, a process which can lead to the formation of many oxygen minimum zones (OMZs) in modern settings. Firstly, the potential for deep, nutrient-rich waters from the wider oceans entering the basin is limited due to the depositional setting within the East Greenland Basin, which was probably divorced from wider oceanic circulation. Any upwelling nutrients in the open Boreal Ocean would most likely have been consumed as they encountered the distal shelf at the mouth of the embayment some 500 km to the north. Secondly, modern OMZs are typically in waters no shallower than ca. 100–200 m (e.g. Levin et al., 2002; Stramma et al., 2010). This is where upwelling nutrients enter the photic zone generating biomass. This bio-material rains to the shelf floor driving BOD and leading to anoxic conditions. In contrast, the site of deposition at Fiskegrav was probably shallower than 100 m.

At Fiskegrav, our Fe speciation ($Fe_{PY}/Fe_{HR} \leq 0.7$) data indicate the establishment of ferruginous conditions in Interval 4, rather than potentially euxinic conditions implied by previous studies (Neilsen et al., 2010; Bond and Wignall, 2010). This apparent discrepancy in redox interpretations may result from the application of different palaeoredox proxies. For example, Neilsen et al. (2010) and Bond and Wignall (2010) employed pyrite framboid size distributions, a method which is based upon the assumption that small framboids (e.g. ca. 5 μm or less) with a small standard deviation are diagnostic of sulphate reduction occurring in the water column (i.e. euxinic conditions). In such cases, pyrite framboid sizes are limited as they can only grow at the oxic-anoxic chemocline for a limited time before gravitational removal from the site of active MSR (Wilkin et al., 1996; Wilkin and Arthur, 2001). The method further assumes that framboids that grow within the sediment pile (under non-euxinic conditions) may grow to much larger sizes, as the sediments can support their mass at the oxic/anoxic interface for more extended periods of time.

However, recent studies indicate that small framboids may not be an unequivocal indicator of water column euxinia. These studies indicate that small framboids may also be the product of processes occurring within the sediments, where rapid sedimentation restricts time spent at the oxic-anoxic interface, and where a paucity of labile electron donors slow MSR rates (Gallego-Torres et al., 2015). High sedimentation rates and low TOC levels at Fiskegrav (Twitchett et al., 2001; Algeo and Twitchett, 2010) may thus have resulted in anomalously small framboids being formed within the sediments. The changes in water-column redox conditions indicated by our Fe speciation data are also broadly consistent with inferred redox changes established during the period around the disappearance of biota from other Boreal sites. For example at Kap Stosch (East Greenland) Pristane/Phytane (Pr/Ph) and C_{35}/C_{34} hopane ratios indicate anoxic conditions, and possibly water-column euxinia, due to the presence of 2,3,6-trimethyl isoprenoids, isorenieratane and crocetane, during the deposition of sediments probably equivalent to the lowermost Wordie Creek Formation (Hays et al., 2012). However, we note that in shallow depositional settings where the photic zone may have reached the sea floor, compounds such as isorenieratane can be generated in microbial mats that oxidise H_2S as it percolates up from the sediments and thus might not be diagnostic of euxinia (Meyer et al., 2011). At Festningen (Svalbard) pyrite framboid size distributions indicate broadly anoxic conditions across the section of outcrop where biota disappear, with the possibility of euxinic conditions some 5 m higher in the section (Bond and Wignall, 2010). Studies of the degree of pyritization and TOC/sulphur ratios (Wignall et al.,

1998) indicate that parts of the Kap Starostin Fm at Festningen may have fluctuated between oxic and euxinic conditions as well. A shift to increased anoxia coincident with the disappearance of biota at Festningen is also inferred from a multi-proxy redox study by Grasby et al. (2015). Another framboid study at Tshermakfjellet (Svalbard) also suggested that the disappearance of bioturbation is consistent with a transition to euxinic conditions (Dustira et al., 2013).

Interrogation of TOC and TN records provides further support for a decline in oxygen availability up-section. Syn-depositional oxidative processes promote the degradation of organic matter, liberating carbon degradation products (CO_2), whilst retaining some nitrogenous products as either ammonium (NH_4^+) adsorbed on to clays or as organic nitrogen (Gao et al., 2012). Consequently, TOC/TN ratios may fall below the Redfield minima (which Meyers (1997) established as ca. 4 for algae and Gao et al. (2012) establish as ca. 5 for marine organic matter) in settings where oxidative degradation of organic matter occurs. This inference is supported further by the observation that lower TOC/TN ratios indicative of oxidative degradation are mostly recorded from bioturbated beds (Figs. 4, 6f; Table S3), where oxidative mineralisation of organic matter would have been enhanced by the activities of bioturbators irrigating the sediment with O_2-bearing waters (Aller 1994; Kristensen, 2000). However, TOC/TN ratios are still close to the Redfield minima in laminated horizons (Figs. 4, 6f; Table S3), which we interpret this as indicating the loss of organic carbon associated with anaerobic respiration, e.g., via microbial nitrate or sulphate reduction (Lückge et al., 1999).

Relatively high TOC/TN ratios are recorded in Interval 1 despite extensive bioturbation and Fe speciation data indicating oxic deposition. Normally we would expect oxygenated depositional environments to be associated with lower organic carbon preservation, leading to lower TOC/TN ratios in bioturbated sediments than in laminated beds, as seen in Interval 2. We suggest that these high TOC/TN ratios in Interval 1 may represent higher inputs of marine organic carbon into the sediments resulting from higher primary productivity in early stages of the extinction event, compared with conditions higher in the section. Alternatively, these values could represent fluxes of dead terrestrial organic matter from the reorganisation of terrestrial vegetation (Looy et al., 2001), along with the initial dieback of marine biota. In principle, sedimentary TOC/TN ratios can also be modified by changes in the detrital flux of clay minerals into the depositional setting, in circumstances where potassium (K^+) in clay minerals has been replaced by ammonium (NH_4^+), either adsorbed onto or incorporated within the structure of minerals (Sterne et al., 1989). However, a significant input of such material is unlikely at Fiskegrav, as no relationship is apparent between K abundance, a proxy for clay input, and TOC/TN (Fig. 6g; $R^2 = 0.01$) (e.g. Saitoh et al., 2014 and references therein).

5.4. Stable isotope biogeochemistry

Our new $\delta^{13}C_{org}$ data (Fig. 4, Table S3, Section 5.4) show a trend towards increasingly negative $\delta^{13}C_{org}$ values up section which can be divided into two phases; first a sharp fall from ca. −24‰ to ca. −27‰, in the 50 cm below Interval 1, followed by a more gradual change to ca. −30‰. Large excursions in the Late Permian $\delta^{13}C_{org}$ marine record, such as that noted here, are reported from around the world. They are, however, a complex phenomenon and could have been influenced by a number of factors. These include the extensive input into the biosphere of ^{13}C-depleted carbon from the eruption of the Siberian Traps along with carbon released during contact metamorphism between the erupting magmas and organic-rich sediments. Additional factors include the possibility of the input into the biosphere of sea-floor methane hydrates, destabilised by increasing global temperatures (Korte and Kozur, 2010 and references therein).

These large shifts towards increasingly negative $\delta^{13}C_{org}$ values could also have been amplified by processes that contributed to the more gradual shift to even lighter $\delta^{13}C_{org}$ values recorded across and above
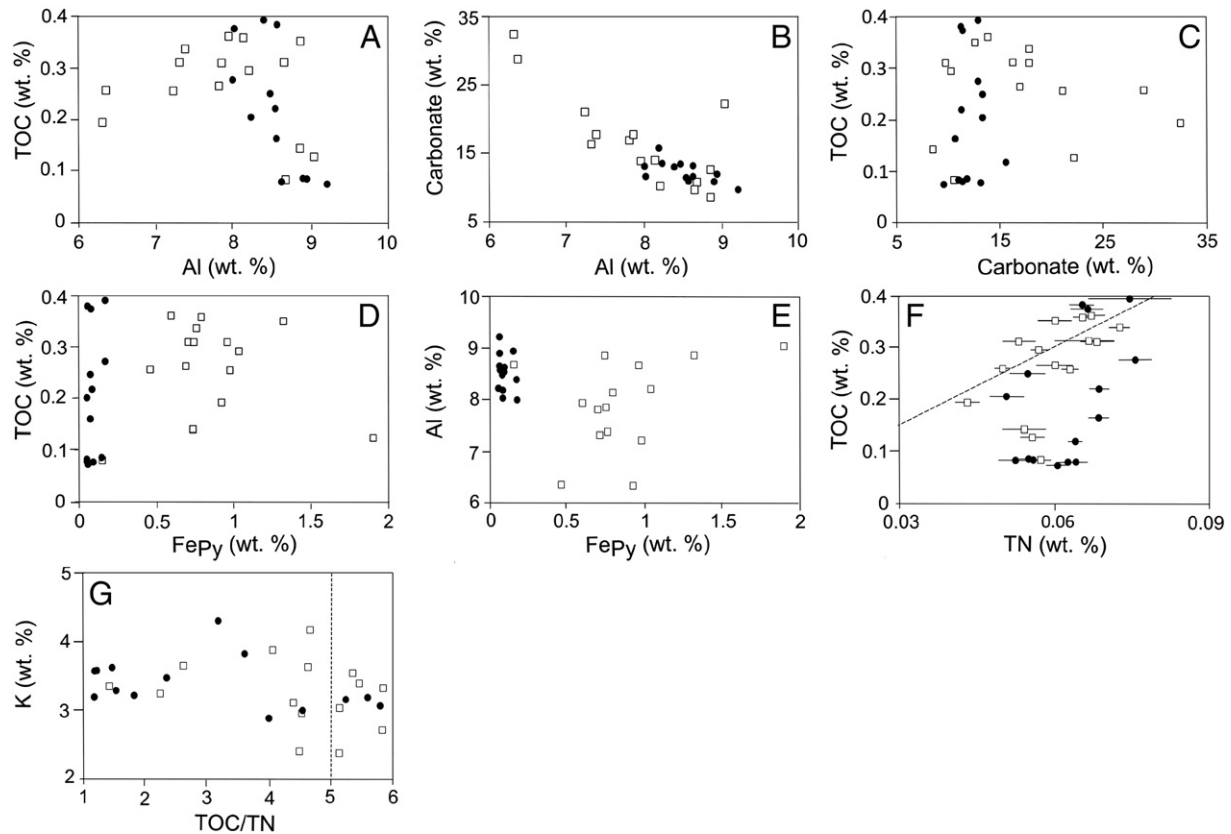
Fig. 6. Cross plots of major elements along with TOC and TN. Dashed line in F and G shows Redfield C/N ratio minimum for organic matter (Gao et al., 2012). In F data plotted below and to right of dashed line shows sub-Redfield ratios, in G data plotted to the left of the dashed line shows sub-Redfield ratios. Open squares represent laminated horizons and filled circles represent bioturbated sediments.

the formational contact. An increase in freshwater input up section could have led to an increase in the proportions of terrestrially derived organic material. However, the effects of such potential changes in the proportions of terrestrial to marine material are difficult to assess. In modern settings there is considerable overlap between the average $\delta^{13}C$ values for marine and terrestrial vegetation, although the $\delta^{13}C$ of marine plants is generally isotopically heavier than that of land plants (Cloern et al., 2002). However, the relative $\delta^{13}C$ values for marine and terrestrial plants prior to the end of the Mesozoic may have been reversed (Arthur et al., 1985). Further, we cannot discount a role for an input of reworked sedimentary organic carbon weathered from the local Palaeozoic hinterland, the isotopic composition of which is unknown, nor the impact of changes in atmospheric pCO_2 causing changes in fractionation effects associated with photosynthesis. Probably the most important factors for the slow decline in $\delta^{13}C$ values are a combination of the incursion of isotopically light deeper water (e.g. Meyer et al., 2016) associated with the transgression and an increase in the anaerobic recycling of carbon during methnogenesis/methnotrophy, or by other the presence of other anaerobic microbes in low-oxygen settings (e.g. Luo et al., 2014).

Declining oxygen availability up section, leading to a fall in rates of oxidative degradation of organic matter, cannot be invoked as a factor influencing a shift towards isotopically lighter $\delta^{13}C_{org}$ values. Whilst increased oxidative degradation can lead to increases in $\delta^{15}N_{org}$ through processes of deamination and decarboxylation (Freudenthal et al., 2001), oxidative degradation of carbon may have the opposite effect and reduce $\delta^{13}C_{org}$ by up to ca. 1.6‰ (Freeman, 2001; Freudenthal et al., 2001; Lehman et al., 2002; Koehler et al., 2017).

The $\delta^{15}N_{bulk}$ values at Fiskegrav (ca. +4‰ to ca. +6‰) are similar to values for modern marine organic matter, which has an average $\delta^{15}N$ value of ca. +5‰ to +6‰ (Sigman et al., 2009). These values are also similar to slightly lower than those reported for Panthalassic sites

(Algeo et al., 2012; Schoepfer et al., 2012; Knies et al., 2013; Grasby et al., 2016) and for the Late Permian of Svalbard (Grasby et al., 2015). These values are inconsistent with evidence for nitrogen limitation (e.g., $\delta^{15}N \leq 0‰$, indicative of N_2 fixation), and probably represent nitrification within a predominantly oxic surface ocean followed by incomplete denitrification within OMZs. Significantly, positive $\delta^{15}N_{bulk}$ values indicative of denitrification provide further evidence that the water column was not euxinic, as nitrate is a more favourable electron acceptor for anaerobic respiration than sulphate, and should be consumed within the water column by denitrification prior to the onset of water column MSR.

Our $\delta^{15}N_{bulk}$ values are higher than values published for Tethyan sections, which generally show declines to values close to 0‰ (e.g. Saitoh et al., 2014; Xiang et al., 2016). These low $\delta^{15}N_{bulk}$ values in Tethyan sections are attributed to enhanced diazotrophy under nitrate-limited conditions (Saitoh et al., 2014). Whilst our $\delta^{15}N_{bulk}$ data does not indicate that nitrate limitation was a factor at Fiskegrav, we do note that the lack of bioturbation in Intervals 2, 3, 4, which we attribute to anoxic conditions, could have imparted some degree of nutrient stress, as ventilation and irrigation of the substrate by bioturbation would normally release sequestrated nutrients for recycling into the overlying water (Hansen and Kristensen, 1997). Fe limitation restricting biological activity, also seems unlikely given that Fe is available in ferruginous conditions, as opposed to euxinic conditions, where it can be titrated from the water column, whilst phosphate limitation is also unlikely in laminated horizons as phosphate is more readily released from sediments in anoxic conditions (Kraal et al., 2010).

Sulphur isotope data from Fiskegrav do, however, support an important role for MSR in organic matter remineralization within the sediments. During the Late Permian, the $\delta^{34}S$ of seawater sulphate in the East Greenland Basin is estimated to have been +11.5‰, as established from evaporitic deposits in the Karstryggen Fm which underlies the

Schuchert Dal Fm (Nielsen and Shen, 2004), and consistent with other Late Permian data (Strauss, 1997; Kaiho et al., 2006; Peryt et al., 2010). Our new $\delta^{34}S_{pyr}$ data mostly range from −44.3 to −34.2‰ (with outliers at −16.4, −1.8 and +43.1‰ as discussed in Section 5.5), in agreement with previously published values (Neilsen et al., 2010). These data imply a fractionation in $\delta^{34}S$ between seawater sulphate and sulphide ($\varepsilon_{SO4 - H2S}$) of between ~46‰ and ~56‰, assuming H_2S is the dominant source of sulphur in pyrite. We interpret these $\delta^{34}S_{pyr}$ values as recording MSR rather than euxinia and/or fractionation effects associated with sulphur oxidation and disproportionation processes (cf. Fenton et al., 2007; Neilsen et al., 2010). Recent work has demonstrated that large fractionations between seawater sulphate and sulphide ($\varepsilon_{SO4 - H2S} \geq 60‰$) can be produced via MSR alone, at low sulphate reaction rates, when organic electron donors are limited (Canfield et al., 2010; Sim et al., 2011). The low TOC values at Fiskegrav support a limited carbon flux to sulphate reducers in the sediments, and could easily support such moderately large fractionations during MSR.

5.5. Fluctuations in depositional conditions and the disappearance of benthos

Superimposed on the overall transgressive event and decline in oxygen availability is a covariation of geochemical fluctuations with changing lithology and bioturbation throughout Interval 2, with the bulk chemical properties of the two lithologies plotting into two distinct populations (Fig. 7). As discussed above (Section 5.2), smaller grain size and low Al coupled to higher TOC, Fe_{PY} and carbonate abundances in laminated horizons, and vice versa for bioturbated horizons, probably reflect redox changes resulting in enhanced preservation of organic matter, MSR, and carbonate precipitation in oxygen restricted laminated layers. The alternations of laminated and bioturbated mudstone in Interval 2 indicate that at times the seafloor was devoid of

benthic animals and at other times supported an infaunal community of micro- and meiofauna, although macroscopic shelly fossils remained absent. Fe speciation data indicate that potentially anoxic conditions ($0.22 \leq Fe_{HR}/Fe_T \leq 0.38$) were prevalent during the deposition of the upper three bioturbated horizons, which may indicate low oxygen availability. However, many modern benthic organisms are able to tolerate dissolved oxygen (DO) levels as low as 1 mg L^{-1} before abandoning their burrows (Levin et al., 2009), or even inhabit hypoxic environments (Braeckman et al., 2013). Further, modern studies indicate that intermittent rises in DO concentrations to around 1 mg L^{-1}, for periods as short as a few weeks or months, may allow temporary access to the substrate for opportunistic benthos (Berge, 1990; Lu and Wu, 2000; Ryu et al., 2010). Once recolonization begins, bioturbation to depths of several centimetres can occur rapidly (Graf, 1989; Pope et al., 1996; Hartmann et al., 2009). We suspect that such short-term small fluctuations in redox conditions against a background of long-term anoxia may be undetectable by the bulk Fe speciation method. In addition, the accumulation of pyrite within the laminated layers is much higher than within bioturbated horizons, possibly due to relatively higher abundances of TOC fuelling more vigorous rates of MSR within these sediments. This could have allowed the build-up of H_2S just beneath the sediment-water interface, rendering the substrate uninhabitable.

Additional geochemical data does, however, support the transient presence of oxygen during the deposition of the upper three bioturbated horizons in Interval 2. Specifically, lower TOC/TN ratios and elevated $\delta^{15}N_{bulk}$ values in the bioturbated horizons in comparison to laminated layers (Figs. 4, 7f; Table S3) indicate *syn*-depositional oxidative degradation (Freudenthal et al., 2001; Möbius et al., 2010; Saitoh et al., 2014). Changes in the relative input of marine and terrestrial organic matter and their influence on $\delta^{15}N_{bulk}$ values are difficult to assess, as there can be a significant overlap between marine and terrestrial
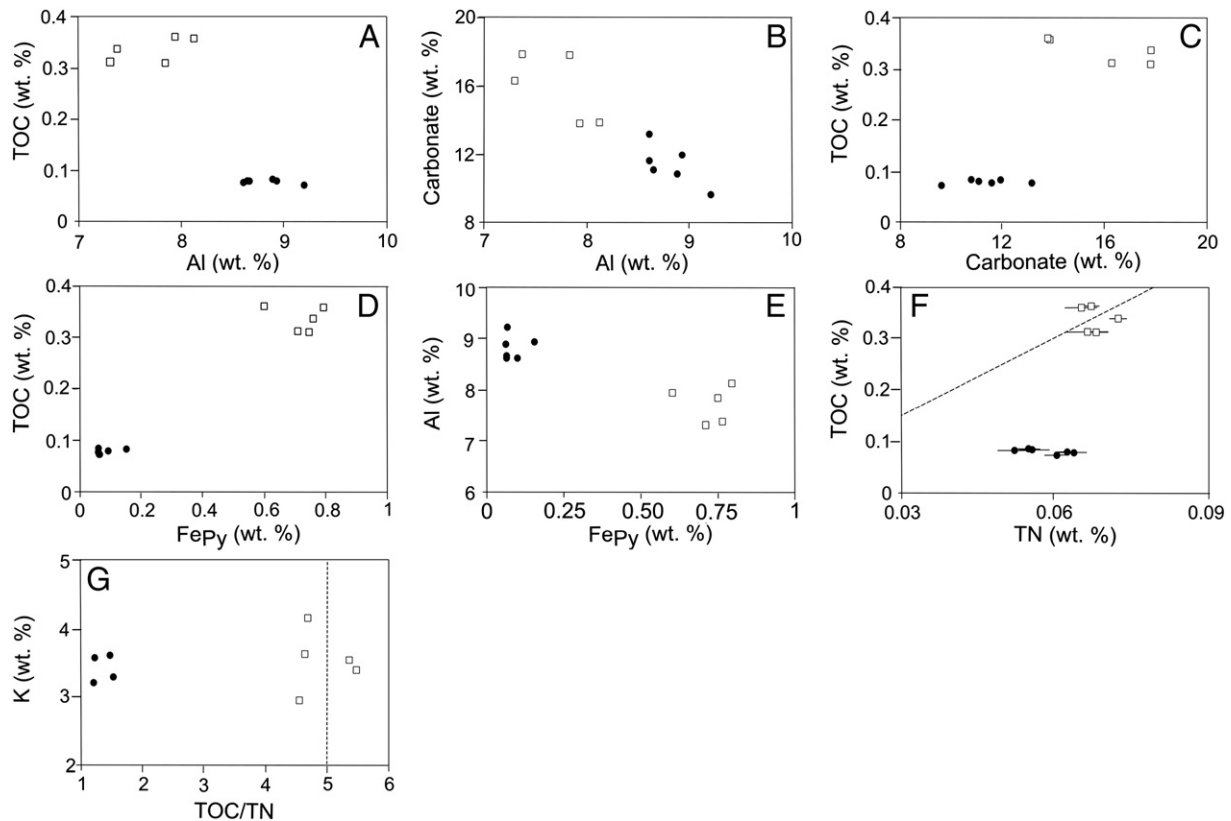

Fig. 7. Cross plots of major elements and TOC and TN in Interval 2 only. Dashed lines in F and G show Redfield C/N ratio minimum for organic matter (Gao et al., 2012). In F, data plotted below and to the right of the dashed line shows sub-Redfield ratios; in G, data plotted to the left of the dashed line shows sub-Redfield ratios. Open squares represent laminated layers and filled circles represent bioturbated horizons.

matter, with the $\delta^{15}N$ of modern terrestrial flora (including saltmarsh plants) ranging from ca. $-4‰$ to ca. $+18‰$ (Schoeninger et al., 1983; Cloern et al., 2002).

Fe speciation data in the laminated unbioturbated horizons of Intervals 2 and 3 are similar to the values measured in the uppermost bioturbated horizons of Interval 2. While this trend suggests that oxygen may have been transiently available during the deposition of these horizons, such putative oxidative events must have been slight and extremely short, precluding the recolonization of the sea bed.

Data from Interval 2 (Fig. 8B) show that bioturbated horizons have slightly higher $\delta^{13}C_{org}$, but significantly lower TOC abundances, than laminated beds. This could imply that $\delta^{13}C_{org}$ values in these horizons are controlled by the oxidative breakdown of organic matter, with labile organic matter being removed from bioturbated horizons leaving the remaining refractory organic matter ^{13}C-enriched. However, as noted above, such processes can actually lead to isotopically lighter $\delta^{13}C_{org}$ values (Meyers, 1994; Freeman, 2001; Freudenthal et al., 2001; Lehman et al., 2002; Koehler et al., 2017). It is possible that such $\delta^{13}C_{org}$ variability is due to variations in the influence of ^{13}C-depleted transgressive deeper waters, produced by periodic upwelling, as has been proposed to explain similar patterns in $\delta^{13}C_{carb}$ values in Late Permian sediments from Nhi Tao, Vietnam (Algeo et al., 2008). However, we would not anticipate this to be the case at Fiskegrav, where we speculate that laminated horizons in Interval 2 are associated with onshore winds, which would preclude upwelling (Section 5.6). Therefore the most likely causes for these small variations in $\delta^{13}C_{org}$ values are methane recycling and the activities of other anaerobic microbes generating ^{13}C-depleted organic matter during the deposition of laminated horizons (e.g. Luo et al., 2014).

Although sulphur isotope ($\delta^{34}S_{pyr}$) values are generally stable, they do show some fluctuations, especially in Interval 2 where $\delta^{34}S_{pyr}$ values are generally higher in bioturbated horizons (Fig. 4, Table S3). Modification of $\delta^{34}S_{pyr}$ values at Fiskegrav has previously been attributed to oxidative recycling of sulphur, but this mechanism should produce increasingly negative $\delta^{34}S_{pyr}$ values in ventilated horizons (Neilsen et al., 2010; Fenton et al., 2007). Differences in $\delta^{34}S_{pyr}$ values could theoretically reflect changes in rates of MSR associated with variations in the abundance and quality of electron acceptors, such as organic carbon (Sim et al., 2011). However, again we might expect the opposite trend to that observed, with smaller $\delta^{34}S$ fractionations in laminated layers where TOC abundances are higher. Closed system sulphate reduction can decrease fractionations during MSR, due to the effects of Rayleigh distillation; however, it is difficult to imagine a scenario whereby bioturbated horizons would be more closed to exchange with overlying seawater than the laminated layers. We also observe extreme ^{34}S–enrichment in one data point, where $\delta^{34}S_{pyr} = +43.1‰$. Such 'superheavy pyrite' values have been reported in modern shallow-water environments and linked to sedimentary reworking and bioturbation (Fike et al., 2015), although the mechanism controlling these ^{34}S enrichments is currently unknown. Given that most of our slightly ^{34}S-enriched $\delta^{34}S_{pyr}$ values are from bioturbated horizons, we suggest

that these values could represent the influence of biologically mediated mixing of reduced and oxidized sediments, partially offsetting the fractionation effects associated with MSR.

5.6. Causes of punctuated redox changes

Depending upon the age constraints we apply for sedimentation rates, the deposition of Interval 2 could represent between 2 kyr and 10 kyr (Section 2.3). These estimates imply that transitions between bioturbated and laminated beds in Interval 2 are on broadly millennial or even centennial timescales. Given the limited information available, we speculate that the most parsimonious explanation for these depositional and redox fluctuations is that they reflect changes in weather patterns resulting from Hadley Cell dynamics. For example, Wang et al. (2007) reveal variations in rainfall intensity in Brazil that have occurred on both millennial and orbital timescales over the last 90 kyr, which they argue could be related to displacement in the mean position of the intertropical convergence zone and associated asymmetry in Hadley Cell characteristics. Additionally, shifts in the latitudinal position of the Southern Westerlies resulting from Hadley Cell dynamics have been implicated in changing weather patterns and millennial-scale changes in sediment characteristics off the west coast of Chile (Lamy et al., 2001). Climatic variations with millennial frequency have also been inferred and identified in other Holocene records (Bond et al., 1997, 2001; Sarnthein et al., 2003; Debret et al., 2007; Santos et al., 2013), in Dansgaard–Oeschger cycles during the Pleistocene (Dansgaard et al. 1993; Grootes and Stuiver, 1997), and also for some Carboniferous and Permian rhythmites, leading to suggestions that such climatic periodicity could be endemic throughout the Phanerozoic (Elrick and Hinnov, 2007; Franco et al., 2012).

If we accept the most rapid sedimentation rates for Fiskegrav, where 1 m is equivalent to ca. 2 kyr, then the fluctuations we see must represent sub-millennial variability. Such climate cyclicity on timescales of between 300 and 700 years have also been identified in the Holocene from a range of latitudes and have been linked to solar forcing, changes in the Earth's magnetic field and/or teleconnections between ocean-atmosphere and ice sheet dynamics (e.g. Gallet et al., 2005; Moberg et al., 2005; Zanchettin et al., 2013; Soon et al., 2014; Xu et al., 2014). We point in particular to a study of the western Mediterranean Sea, at latitude 36°N, broadly similar to the latitude of Fiskegrav in the Permian, where millennial and sub-millennial climate variability has been invoked to explain changes in sediment transport, including wind-blown dust and fluvial runoff, along with changes in marine productivity and redox conditions (Rodrigo-Gámiz et al., 2014). However, we note that the probable lack of polar ice during the Permian implies that some of the teleconnections and mechanisms controlling climate fluctuations in the Permian may be different to those in the Holocene.

We speculate that the putative expansion of the Hadley Cell during the Late Permian (Section 5.3) was complex and oscillatory upon millennial or shorter timescales. Changes during the deposition of
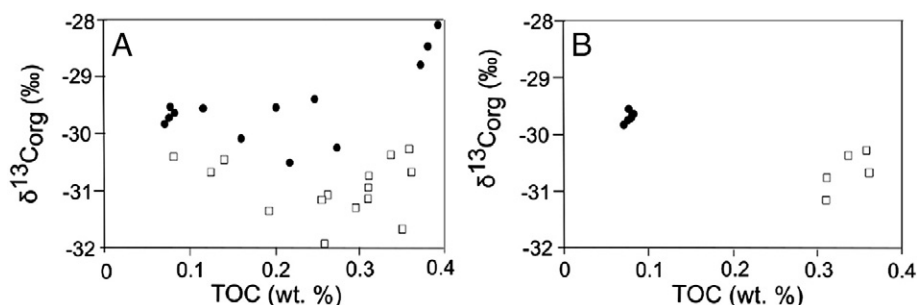

Fig. 8. Cross plots $\delta^{13}C_{org}$ and TOC for whole section (A) and Interval 2 only (B). Open squares represent laminated layers and filled circles represent bioturbated horizons.

Interval 2 possibly reflect changes between predominantly onshore winds and offshore winds. When under the influence of the Hadley Cell (Fig. 5B, C), increased precipitation and runoff could have enhanced water column stratification, thus restricting mixing during the deposition of laminated horizons. Simultaneously, enhanced fluxes of freshwater could have delivered additional nutrients from the hinterland, thus stimulating BOD. In contrast, periods of offshore winds and resultant rain shadow effects under Mid-Latitude influence (Fig. 5A, C) could have led to lessened freshwater input. This climate regime could have reduced salinity stratification, with smaller nutrient fluxes simultaneously leading to reduced BOD at the ocean floor.

Following this scenario, the disappearance of intermittent recolonization at the top of Interval 2 could indicate that the northwards expansion of the Hadley Cell boundary meant that deposition at Fiskegrav was decreasingly influenced by climatic fluctuations and onshore winds, and increased runoff gradually became the norm. However, we do note some continued geochemical fluctuations within Intervals 3 and 4, suggesting that these climatic variations could have continued more sporadically. By this time, a general transgression could have resulted in depositional conditions deep enough that climatic forcing had a declining influence on sedimentary processes at the sea floor, and more persistent anoxia precluded recolonization.

6. Conclusions

Sedimentological and geochemical evidence from the upper Schuchert Dal and lower Wordie Creek formations at Fiskegrav demonstrate that the collapse of the Late Permian shallow shelf ecosystem and the cessation of bioturbation occurred during a marine transgression and under progressively more oxygen-deficient conditions. Declining oxygen availability is attributed to the transgressive shoreward expansion of oxygen deficient waters, and the possible intensification of BOD resulting from increased delivery of terrestrially derived nutrients and water column stratification. During this change the water column was characterised by a shift from oxic to ferruginous depositional conditions.

A lack of evidence for euxinic conditions (Fe speciation and $\delta^{34}S_{pyr}$) is supported by $\delta^{15}N_{bulk}$ data that is indicative of nitrate availability, which could have provided a more energetically favourable electron acceptor than sulphate for anaerobic respiration in the water column. These $\delta^{15}N_{bulk}$ data also imply that nitrate-limitation was not a significant factor contributing to the extinction or recovery of marine organisms at Fiskegrav, although periods without bioturbation may have reduced the recycling of nutrients from the sediments.

Fluctuations in geochemistry and sedimentology throughout the middle part of the section record a dynamic depositional setting that fluctuated between periods of reduced oxygen availability, where benthic colonisation was prevented, and periods of oxygenation, when some bioturbation occurred, probably by an infaunal meiobenthos. Given the temporal frequency of these events, which appear to match the proposed millennial- or centennial-scale timings of Palaeozoic, Pleistocene and Holocene environmental cyclicity, the primary mechanism driving these events was probably climatic forcing which generated relative high-frequency changes in precipitation and ultimately nutrient delivery to the shelf.

Supplementary data to this article can be found online at http://dx.doi.org/10.1016/j.palaeo.2017.06.014.

References

Algeo, T.J., Twitchett, R.J., 2010. Anomalous Early Triassic sediment fluxes due to elevated weathering rates and their biological consequences. Geology 38, 1023–1026.

Algeo, T.J., Shen, Y., Zhang, T.G., Lyons, T.W., Bates, S., Rowe, H., Nguyen, T.K.T., 2008. Association of ^{34}S-depleted pyrite layers with negative carbonate $\delta^{13}C$ excursions at the Permian–Triassic boundary: evidence for upwelling of sulfidic deep-ocean water masses. Geochem. Geophys. Geosyst. http://dx.doi.org/10.1029/2007GC001823.

Algeo, T., Chen, Z.Q., Fraiser, M.L., Twitchett, R.J., 2011. Terrestrial–marine teleconnections in the collapse and rebuilding of Early Triassic marine ecosystems. Palaeogeogr. Palaeoclimatol. Palaeoecol. 308, 1–11.

Algeo, T., Henderson, C.M., Ellwood, B., Rowe, H., Elswick, E., Bates, S., Lyons, T., Hower, J.C., Smith, C., Maynard, B., Hays, L.E., Summons, R.E., Fulton, J., Freeman, K.H., 2012. Evidence for a diachronous Late Permian marine crisis from the Canadian Arctic region. Geol. Soc. Am. Bull. 124, 1424–1448.

Aller, R.C., 1994. Bioturbation and remineralization of sedimentary organic matter: effects of redox oscillation. Chem. Geol. 114, 331–345.

Arthur, M.A., Dean, W.E., Claypool, G.E., 1985. Anomalous ^{13}C enrichment in modern marine organic carbon. Nature 315, 216–218.

Benton, M.J., Twitchett, R.J., 2003. How to kill (almost) all life: the end-Permian extinction event. Trends Ecol. Evol. 18, 358–365.

Berge, J.A., 1990. Macrofauna recolonization of subtidal sediments. Experimental studies on defaunated sediment contaminated with crude oil in two Norwegian fjords with unequal eutrophication status. I. Community responses. Mar. Ecol. Prog. Ser. 66, 103–115.

Black, B.A., Hauric, E.H., Elkins-Tanton, L.T., Brown, S.M., 2014. Sulfur isotopic evidence for sources of volatiles in Siberian Traps magmas. Earth Planet. Sci. Lett. 394, 58–69.

Bond, D.P.G., Wignall, P.B., 2010. Pyrite framboid study of marine Permian–Triassic boundary sections: a complex anoxic event and its relationship to contemporaneous mass extinction. Geol. Soc. Am. Bull. 122, 1265–1279.

Bond, G., Showers, W., Cheseby, M., Lotti, R., Almasi, P., de Menocal, P., Priore, P., Cullen, H., Hajdas, I., Bonani, G., 1997. A pervasive millennial-scale cycle in North Atlantic Holocene and Glacial climates. Science 278, 1257–1266.

Bond, G., Kromer, B., Beer, J., Muscheler, R., Evans, M.N., Showers, W., Hoffmann, S., Lotti-Bond, R., Hajdas, I., Bonani, G., 2001. Persistent solar influence on North Atlantic climate during the Holocene. Science 294, 2130–2136.

Böttcher, M.E., 2011. Manganese (Sedimentary Carbonates and Sulfides). In: Reitner, J., Thiel, V. (Eds.), Encyclopedia of Geobiology. Springer, pp. 541–542.

Bottjer, D.J., Clapham, M.E., Frasier, M.L., Powers, C.M., 2008. Understanding mechanisms for the end-Permian mass extinction and the protracted Early Triassic aftermath and recovery. GSA Today 18, 4–10.

Bowring, S.A., Erwin, D.H., Jin, Y.G., Martin, M.W., David, K., Wang, W., 1998. U/Pb zircon geochronology and tempo of the end-Permian mass extinction. Science 280, 1039–1045.

Braeckman, U., Vanaverbeke, J., Vincx, M., van Oevelen, D., Soetaert, K., 2013. Meiofauna metabolism in suboxic sediments: currently overestimated. PLoS One. http://dx.doi.org/10.1371/journal.pone.0059289 (March 28).

Burgess, S.D., Bowring, S., Shen, S.-Z., 2014. High-precision timeline for Earth's most severe extinction. PNAS 111, 3316–3321.

Canfield, D.E., Raiswell, R., Westrich, J.T., Reaves, C.M., Berner, R.A., 1986. The use of chromium reduction in the analysis of reduced inorganic sulfur in sediments and shales. Chem. Geol. 54, 149–155.

Canfield, D.E., Farquhar, J., Zerkle, A.L., 2010. High isotope fractionations during sulfate reduction in a low-sulfate euxinic ocean analog. Geology 38, 415–418.

Clarkson, M.O., Poulton, S.W., Guilbaud, R., Wood, R.A., 2014. Assessing the utility of Fe/Al and Fe-speciation to record water column redox conditions in carbonate-rich sediments. Chem. Geol. 382, 111–122.

Clarkson, M.O., Wood, R.A., Poulton, S.W., Richoz, S., Newton, R.J., Kasemann, S.A., Bowyer, F., Krystyn, L., 2016. Dynamic anoxic ferruginous conditions during the end-Permian mass extinction and recovery. Nat. Commun. http://dx.doi.org/10.1038/ncomms12236.

Cloern, J.E., Canuel, E.A., Harris, D., 2002. Stable carbon and nitrogen isotope composition of aquatic and terrestrial plants of the San Francisco Bay estuarine system. Limnol. Oceanogr. 47, 713–729.

Dansgaard, W.S., Johnsen, J., Clausen, H.B., Dahl-Jensen, D., Gundestrup, N.S., Hammer, C.U., Hvidberg, C.S., Steffensen, J.P., Sveinbjörnsdottir, A.E., Jouzel, J., Bond, G., 1993. Evidence for general instability of past climate from a 250-kyr ice-core record. Nature 364, 218–220.

Debret, M., Bout-Roumazeilles, V., Grousset, F., Desmet, M., McManus, J.F., Massei, N., Sebag, D., Petit, J.-R., Copard, Y., Trentesaux, A., 2007. The origin of the 1500-year climate cycles in Holocene North-Atlantic records. Clim. Past 3, 569–575.

Doré, A.G., 1991. The structural foundation and evolution of Mesozoic seaways between Europe and the Arctic. Palaeogeogr. Palaeoclimatol. Palaeoecol. 87, 441–492.

Dustira, A.M., Wignall, P.B., Joachimski, M., Blomeier, D., Hartkopf-Fröder, C., Bond, D.P.G., 2013. Gradual onset of anoxia across the Permian–Triassic boundary in Svalbard, Norway. Palaeogeogr. Palaeoclimatol. Palaeoecol. 374, 303–313.

Elrick, M., Hinnov, L.A., 2007. Millennial-scale paleoclimate cycles recorded in widespread Palaeozoic deeper water rhythmites of North America. Palaeogeogr. Palaeoclimatol. Palaeoecol. 243, 348–372.

Erwin, D.H., 2006. Extinction: How Life on Earth Nearly Died 250 Million Years Ago. Princeton University Press, Princeton, New Jersey.

Fenton, S., Grice, K., Twitchett, R.J., Böttcher, M.E., Looy, C.V., Nabbefeld, B., 2007. Changes in biomarker abundances and sulphur isotopes of pyrite across the Permian-Triassic (P/Tr) Schuchert Dal section (East Greenland). Earth Planet. Sci. Lett. 262, 230–239.

Fike, D.A., Bradley, A.S., Rose, C.V., 2015. Rethinking the ancient sulfur cycle. Annu. Rev. Earth Planet. Sci. 43, 593–622.

Foster, W.J., Twitchett, R.J., 2014. Functional diversity of marine ecosystems after the Late Permian mass extinction event. Nat. Geosci. 7, 233–238.

Franco, D.R., Hinnov, L.A., Ernesto, M., 2012. Millenial-scale climate cycles in Permian-Carboniferous rhythmites: permanent feature throughout geologic time? Geology 40, 19–22.

Freeman, K.H., 2001. Isotopic biogeochemistry of Marine organic carbon. In: Valley, J.W., Cole, D.R. (Eds.), Reviews in Mineralogy and Geochemistry. Stable Isotope Geochemistry. Mineralogical Society of America.

Freudenthal, T., Wagner, T., Weinzhöffer, F., Zabel, M., Wefer, G., 2001. Early diagenesis of organic matter from sediments of the eastern subtropical Atlantic: evidence from stable nitrogen and carbon isotopes. Geochim. Cosmochim. Acta 65, 1795–1808.

Friedrich, J., et al., 2014. Investigating hypoxia in aquatic environments: diverse approaches to addressing a complex phenomenon. Biogeosciences 11, 1215–1259.

Gallego-Torres, D., Reolid, M., Nieto-Moreno, V., MartÍnez-Casado, F.J., 2015. Pyrite framboid size distribution as a record for relative variations in sedimentation rate: an example on the toarcian oceanic anoxic event in south Iberian Palaeomargin. Sediment. Geol. 330, 59–73.

Gallet, Y., Genevey, A., Fluteau, F., 2005. Does Earth's magnetic field secular variation control centennial climate change? Earth Planet. Sci. Lett. 236, 339–347.

Gao, X., Yang, Y., Wang, C., 2012. Geochemistry of organic carbon and nitrogen in surface sediments of coastal Bohai Bay inferred from their ratios and stable isotopic signatures. Mar. Pollut. Bull. 64, 1148–1155.

Glennie, K., Higham, J., Stemmerik, I., 2003. Permian. In: Evans, D., Graham, C., Armour, A., Bathurst, P. (Eds.), The Millennium Atlas: Petroleum Geology of the Central And Northern North Sea. Geol. Soc. London, pp. 91–103.

Graf, G., 1989. Benthic-pelagic coupling in a deep-sea community. Nature 341, 437–439.

Grasby, S.E., Beauchamp, B., 2008. Intrabasin variability of the carbon-isotope record across the Permian–Triassic transition, Sverdrup Basin, Arctic Canada. Chem. Geol. 253, 141–150.

Grasby, S.E., Beauchamp, B., 2009. Latest Permian to Early Triassic basin-to-shelf anoxia in the Sverdrup Basin, Arctic Canada. Chem. Geol. 264, 232–246.

Grasby, S.E., Saniei, H., Beauchamp, B., 2011. Catastrophic dispersion of coal fly ash into oceans during the latest Permian extinction. Nat. Geosci. 4, 104–107.

Grasby, S.E., Beauchamp, B., Bond, D.P.G., Wignall, P.B., Talavera, C., Galloway, J.M., Piepjohn, K., Reinhardt, L., Blomeier, D., 2015. Progressive environmental deterioration in northwestern Pangea leading to the latest Permian extinction. GSA Bull. 127, 1331–1347.

Grasby, S.E., Beauchamp, B., Knies, J., 2016. Early Triassic productivity crises delayed recovery from world's worst mass extinction. Geology 44, 779–782.

Grasby, S.E., Shen, W., Yin, R., Gleason, J.D., Blum, J.D., Lepak, Ryan F., Hurley, J.P., Beauchamp, B., 2017. Isotopic signatures of mercury contamination in latest Permian oceans. Geology 45, 55–58.

Grice, K., Cao, C., Love, G.D., Böttcher, M.E., Twitchett, R.J., Grosjean, E., Summons, R.E., Turgeon, S.C., Dunning, W., Jin, Y.G., 2005. Photic zone euxinia during Permian – Triassic superanoxic event. Science 307, 706–709.

Grootes, P.M., Stuiver, M., 1997. Oxygen 18/16 variability in Greenland snow and ice with 10^{-3} to 10^{-5} year time resolution. J. Geophys. Res. 102, 455–470.

Hansen, K., Kristensen, E., 1997. Impact of Macrofaunal recolonization on benthic metabolism and nutrient fluxes in a shallow marine sediment previously overgrown with macroalgal mats. Estuar. Coast. Shelf Sci. 45, 613–628.

Haq, B.U., Schutter, S.R., 2008. A chronology of Paleozoic sea-level changes. Science 322, 64–68.

Hartmann, V.A., Briggs, K., Shivarudrappa, S., Yeager, K.M., Diaz, R., 2009. The impact of hypoxia on bioturbation rates in the Louisiana Continental Shelf, Northern Gulf of Mexico. Proc. IEEE/MTS Oceans '09, Biloxi, MS.

Hays, L.E., Grice, K., Foster, C.B., Summons, R.E., 2012. Biomarker and isotopic trends in a Permian–Triassic sedimentary section at Kap Stosch, Greenland. Org. Geochem. 43, 67–82.

Hovland, M., Talbot, M.R., Qvale, H., Olaussen, S., Aasberg, L., 1987. Methane-related carbonate cements in pockmarks of the North Sea. J. Sed. Res. (SEPM).

Isozaki, Y., 1997. Permo-Triassic boundary superanoxia and stratified superocean: records from lost Deep Sea. Science 276, 235–238.

Izon, G., Zerkle, A.L., Williford, K.H., Farquhar, J., Poulton, S.W., Claire, M.W., 2017. Biological regulation of atmospheric chemistry en route to planetary oxygenation. P.N.A.S. 114, E2571–E2579. http://dx.doi.org/10.1073/pnas.1618798114.

Joachimski, M.M., Lai, X., Shen, S., Jiang, H., Luo, G., Chen, B., Chen, J., Sun, Y., 2012. Climate warming in the latest Permian and the Permian–Triassic mass extinction. Geology 40, 195–198.

Kaiho, K., Chenb, Z.-Q., Kawahatac, H., Kajiwarad, Y., Satoc, H., 2006. Close-up of the end-Permian mass extinction horizon recorded in the Meishan section, South China: sedimentary, elemental, and biotic characterization and a negative shift of sulfate sulfur isotope ratio. Palaeogeogr. Palaeoclimatol. Palaeoecol. 239, 396–405.

Kang, S.M., Lu, J., 2012. Expansion of the Hadley cell under global warming: winter versus summer. J. Clim. 25. http://dx.doi.org/10.1175/JCLI-D-12-00323.1.

Knies, J., Grasby, S.E., Beauchamp, B., Schubert, C.J., 2013. Water mass denitrification during the latest Permian extinction in the Sverdrup Basin, Arctic Canada. Geology 41, 167–170.

Koehler, M.C., Stüeken, E.E., Kipp, M.A., Buick, R., Knoll, A.H., 2017. Spatial and temporal trends in Precambrian nitrogen cycling: a Mesoproterozoic offshore nitrate minimum. Geochim. Cosmochim. Acta 198, 315–337.

Korte, C., Kozur, H.W., 2010. Carbon-isotope stratigraphy across the Permian-Triassic boundary: a review. J. Asian Earth Sci. 39, 215–235.

Kraal, P., Slomp, C.P., de Lange, G.J., 2010. Sedimentary organic carbon to phosphorus ratios as a redox proxy in Quaternary records from the Mediterranean. Chem. Geol. 277, 167–177.

Kreiner-Møller, M., Stemmerik, L., 2001. Upper Permian lowstand fans of the Bredehorn Member, Schuchert Dal Formation, East Greenland. In: Martinsen, O.J., Dreyer, T. (Eds.), Sedimentary Environments Offshore Norway – Palaeozoic to Recent. Norwegian Petroleum Society.

Kristensen, E., 2000. Organic matter diagenesis at the oxic/anoxic interface in coastal marine sediments, with emphasis on the role of burrowing animals. Hydrobiologia 426, 1–24.

Lamy, F., Hebbeln, D., Roehl, U., Wefer, G., 2001. Holocene rainfall variability in southern Chile: a marine record of latitudinal shifts of the southern westerlies. Earth Planet. Sci. Lett. 185, 369–382.

Lau, K.V., Maher, K., Altiner, D., Kelley, B.M., 2016. Marine anoxia and delayed Earth system recovery after the end-Permian extinction. PNAS 113, 2360–2365.

Lehmann, M.F., Bernasconi, S.M., Barbieri, A., McKenzie, J.A., 2002. Preservation of organic matter and alteration of its carbon and nitrogen isotope composition during simulated and in situ early sedimentary diagenesis. Geochim. Cosmochim. Acta 66, 3573–3584.

Levin, L.A., Ekau, W., Gooday, A.J., Jorissen, E., Middelburg, J.J., Naqvi, S.W.A., Neira, C., Rabalais, N.N., 2009. Effects of natural and human-induced hypoxia on coastal benthos. Biogeosciences 6, 2063–2098.

Levin, L.A., 2002. Deep-ocean life where oxygen is scarce. American Scientist 90, 436–444.

Looy, C.V., Twitchett, R.J., Dilcher, D.L., Van Konijnenburg-Van Cittert, J.H.A., Visscher, H., 2001. Life in the end-Permian dead zone. PNAS 98, 7879–7883.

Lu, L., Wu, R.S.S., 2000. An experimental study on recolonization and succession of marine macrobenthos in defaunated sediment. Mar. Biol. 136, 291–302.

Lu, J., Vecchi, G.A., Reichler, T., 2007. Expansion of the Hadley cell under global warming. Geophys. Res. Lett. 34, L06805. http://dx.doi.org/10.1029/2006GL028443.

Lückge, A., Ercegovac, M., Strauss, H., Littke, R., 1999. Early diagenetic alteration of organic matter by sulfate reduction in Quaternary sediments from the northeastern Arabian Sea. Mar. Geol. 158, 1–13.

Luo, G., Algeo, T.J., Huang, J., Zhou, W., Wang, Y., Yang, H., Richoz, S., Xie, S., 2014. Vertical $\delta^{13}C_{Org}$ gradients record changes in planktonic microbial community composition during the end-Permian mass extinction. Palaeogeogr. Palaeoclimatol. Palaeoecol. 396, 119–131.

Lyons, T.W., Severmann, S., 2006. A critical look at iron paleoredox proxies: new insights from modern euxinic marine basins. Geochim. Cosmochim. Acta 70, 5698–5722.

Matear, R.J., Hirst, A.C., 2003. Long-term changes in dissolved oxygen concentrations in the ocean caused by protracted global warming. Glob. Biogeochem. Cycles:17. http://dx.doi.org/10.1029/2002GB001997.

Meyer, K.M., Macalady, J.L., Fulton, J.M., Kump, L.R., Schaperdoth, I., Freeman, K.H., 2011. Carotenoid biomarkers as an imperfect reflection of the anoxygenic phototrophic community in meromictic Fayetteville Green Lake. Geobiology 9, 321–329.

Meyer, K.A., Ridgewell, A., Payne, J.L., 2016. The influence of the biological pump on ocean chemistry: implications for long-term trends in marine redox chemistry, the global carbon cycle, and marine animal ecosystems. Geobiology 14, 207–219.

Meyers, P.A., 1994. Preservation and elemental and isotopic source identification of sedimentary organic matter. Earth Planet. Sci. Lett. 74, 13–26.

Meyers, P.A., 1997. Organic geochemical proxies of paleoceanographic, paleolimnologic, and paleoclimatic processes. Org. Geochem. 27, 213–250.

Moberg, A., Sonechkin, D.M., Holmgren, K., Datsenko, N.M., Wibjörn, K., 2005. Highly variable Northern Hemisphere temperatures reconstructed from low- and high-resolution proxy data. Nature 433, 613–617.

Möbius, J., Lahajnar, N., Emeis, K.-C., 2010. Diagenetic control of nitrogen isotope ratios in Holocene sapropels and recent sediments from the Eastern Mediterranean Sea. Biogeosciences 7, 3901–3914.

Müller, R., Nystuen, J.P., Eide, F., Lie, H., 2005. Late Permian to Triassic basin infill history and palaeogeography of the Mid-Norwegian shelf – East Greenland region. In: Wandas, et al. (Eds.), Onshore-Offshore Relationships on the North Atlantic Margin. NPF special publication Vol. 12, pp. 165–189.

Nabbefeld, B., Grice, K., Schimmelmann, A., Sauer, P.E., Böttcher, M.E., Twitchett, R.J., 2010. Significance of $\delta D_{kerogen}$, $\delta^{13}C_{kerogen}$ and $\delta^{34}S_{pyrite}$ from several Permian/Triassic (P/Tr) sections. Earth Planet. Sci. Lett. 295, 21–29.

Neilsen, J.K., Shen, Y., Piasecki, S., Stemmerik, L., 2010. No abrupt change in redox condition caused the end-Permian marine ecosystem collapse in the East Greenland Basin. Earth Planet. Sci. Lett. 291, 32–38.

Nielsen, J.K., Shen, Y., 2004. Evidence for sulfidic deep water during the Late Permian in the East Greenland Basin. Geology 32, 1037–1040.

Oberhänsli, H., Hsü, K.J., Piasecki, S., Weissert, H., 1989. Permian-Triassic carbon-isotope anomaly in Greenland and in the southern alps. Hist. Biol. 2, 37–49.

Peckmann, J., Reimer, A., Luth, U., Luth, C., Hansen, B.T., Heinicke, C., Hoefs, J., Reitner, J., 2001. Methane-derived carbonates and authigenic pyrite from the northwestern Black Sea. Mar. Geol. 177, 129–150.

Peryt, T.M., Halas, S., Hryniv, S.P., 2010. Sulphur and oxygen isotope signatures of late Permian Zechstein anhydrites, West Poland: seawater evolution and diagenetic constraints. Geol. Quart. 54, 387–400.

Polissar, P.J., Fulton, J.M., Junium, C.K., Turich, Courtney C., Freeman, K.H., 2009. Measurement of ^{13}C and ^{15}N isotopic composition on nanomolar quantities of C and N. Anal. Chem. 81, 755–763.

Pope, R.H., Demaster, D.J., Smith, C.R., Seltman Jr., H., 1996. Rapid bioturbation in equatorial Pacific sediments: evidence from excess [234]Th measurements. Deep-Sea Res. II 43, 1339–1364.

Poulton, S.W., Canfeld, D.E., 2011. Ferruginous conditions: a dominant feature of the ocean through Earth's history. Elements 7, 107–112.

Poulton, S.W., Canfield, D.E., 2005. Development of a sequential extraction procedure for iron: implications for iron partitioning in continentally derived particulates. Chem. Geol. 214, 209–221.

Poulton, S.W., Henkel, S., März, C., Urquhart, H., Flögel, S., Kasten, S., Sinninghe Damsté, J.S., Wagner, T., 2015. A continental-weathering control on orbitally driven redox-nutrient cycling during Cretaceous Oceanic Anoxic Event 2. Geology 43, 963–966.

Raiswell, R., Newton, R., Bottrell, S.H., 2008. Turbidite depositional influences on the diagenesis of Beecher's Trilobite Bed and the Hunsruck Slate; sites of soft tissue pyritization. Am. J. Sci. 308, 105–129.

Reichow, M.K., Pringle, M.S., Al'Mukhamedov, A.I., Allen, M.B., Andreichev, V.L., Buslov, M.M., Davies, C.E., Fedoseev, G.S., Fitton, J.G., Inger, S., Medvedev, A.Ya., Mitchell, C., Puchkov, V.N., Safonova, I.Yu., Scott, R.A., Saunders, A.D., 2009. The timing and extent of the eruption of the Siberian Traps large igneous province: implications for the end-Permian environmental crisis. Earth Planet. Sci. Lett. 277, 9–20.

Riccardi, A.L., Arthur, M.A., Kump, L.R., 2006. Sulfur isotopic evidence for chemocline upward excursions during the end-Permian mass extinction. Geochim. Cosmochim. Acta 70, 5740–5752.

Rodrigo-Gámiz, M., Martínez-Ruiz, F., Rodríguez-Tovar, F.J., Jiménez-Espejo, F.J., Pardo-Igúzquiza, E., 2014. Millennial- to centennial-scale climate periodicities and forcing mechanisms in the westernmost Mediterranean for the past 20,000 yr. Quat. Res. 81, 78–93.

Rothwell, R.G., 1989. Minerals and Mineraloids in Marine Sediments: an Optical Identification Guide. Elsevier Applied Science, London.

Ryu, J., Kim, C.K., Khim, J.S., Park, K.-H., Lee, C.-H., Lee, J.-H., Moon, S.-D., Lee, J.-S., Shim, W., Shim, W.J., Lim, U.-H., Hong, S.H., Song, S.J., Lee, K.-T., 2010. Initial recolonization of benthic fauna in defaunated sediment contaminated with octylphenol: field microcosm exposure study. Toxicol. Environ. Heal. Sci. 2, 132–140.

Saitoh, M., Ueno, Y., Nishizawa, M., Isozaki, Y., Takai, K., Yao, J., Ji, Z., 2014. Nitrogen isotope chemostratigraphy across the Permian-Triassic boundary at Chaotian, Sichuan, South China. J. Asian Earth Sci. 93, 113–128.

Santos, T.P., Franco, D.R., Barbosa, C.F., Belem, A.L., Dokken, T., Albuquerque, A.L.S., 2013. Millennial- to centennial-scale changes in sea surface temperature in the tropical South Atlantic throughout the Holocene. Palaeogeogr. Palaeoclimatol. Palaeoecol. 392, 1–8.

Sarnthein, M., van Kreveld, S.A., Erlenkeuser, H., Grootes, P.M., Kucera, M., Pflaumann, U., Schulz, M., 2003. Centennial-to-millennial-scale periodicities of Holocene climate and sediment injections off western Barents shelf, 75°N. Boreas 32, 447–461.

Schoeninger, M.J., De Niro, M.J., Tauber, H., 1983. Stable nitrogen isotope ratios of bone collagen reflect marine and terrestrial components of prehistoric human diet. Science 220, 1381–1383.

Schoepfer, S.D., Henderson, C.M., Garrison, G.H., Ward, P.D., 2012. Cessation of a productive coastal upwelling system in the Panthalassic Ocean at the Permian–Triassic boundary. Palaeogeogr. Palaeoclimatol. Palaeoecol. 313-314, 181–188.

Seidler, L., Steel, R.J., Stemmerik, L., Surlyk, F., 2004. North Atlantic marine rifting in the Early Triassic: new evidence from East Greenland. J. Geol. Soc. Lond. 161, 583–592.

Shen, S.-Z., et al., 2011. Calibrating the end-Permian mass extinction. Science 334, 1367–1372.

Shen, J., Feng, Q., Algeo, T.J., Li, C., Planavsky, N.J., Zhou, L., Zhang, M., 2016. Two pulses of oceanic environmental disturbance during the Permian–Triassic boundary crisis. Earth Planet. Sci. Lett. 443, 139–152.

Siesser, W.G., Rogers, J., 1976. Authigenic pyrite and gypsum in South West African continental slope sediments. Sedimentology 23, 567–577.

Sigman, D.M., Karsh, K.L., Casciotti, K.L., 2009. Ocean process tracers: Nitrogen isotopes in the ocean. In: Steele, J.H., Turekian, K.K. (Eds.), Encyclopedia of Ocean Sciences. Academic Press, London.

Sim, M.S., Bosak, T., Ono, S., 2011. Large sulfur isotope fractionation does not require disproportionation. Science 333, 74–77.

Song, H., Wignall, P.B., Chu, D., Tong, J., Sun, Y., Song, H., He, W., Tian, L., 2014. Anoxia/high temperature double whammy during the Permian-Triassic marine crisis and its aftermath. Sci Rep 4, 4132.

Soon, W., Herrera, V.M.V., Selvaraj, K., Traversi, R., Usoskin, I., Chen, C.-T.A., Lou, J.-Y., Kao, S.-J., Carter, R.M., Pipin, V., Severi, M., 2014. A review of Holocene solar-linked climatic variation on centennial to millennial timescales: physical processes, interpretative frameworks and a new multiple cross-wavelet transform algorithm. Earth Sci. Rev. 134, 1–15.

Stemmerik, L., Christiansen, F.G., Piasecki, S., Jordt, B., Marcussen, C., Nøhr-Hansen, H., 1993. Depositional history and petroleum geology of the Carboniferous to Cretaceous sediments in the northern part of East Greenland. In: Vorren, T.O., Bergsager, E., Dahl-Stamnes, Ø.A., Holter, E., Johansen, B., Lie, E., Lund, T.B. (Eds.), Arctic Geology and Petroleum Potential. Norwegian Petroleum Society (NPF), Special Publication, p. 2.

Stemmerik, L., Bendix-Almgreen, S.E., Piasecki, S., 2001. The Permian-Triassic boundary in central East Greenland: past and present views. Geol. Soc. Denmark Bull. 48, 159–167.

Sterne, E.J., Reynolds, R.C., Zantop, H., 1989. Natural ammonium illites from black shales hosting a stratiform base metal deposit, Delong Mountains, northern Alaska. Clay Clay Miner. 30, 161–166.

Stramma, L., Schmidtko, S., Levin, L.A., Johnson, G.C., 2010. Ocean oxygen minima expansions and their biological impacts. Deep-Sea Res. I 57, 587–595.

Strauss, H., 1997. The isotopic composition of sedimentary sulphur through time. Palaeogeogr. Palaeoclimatol. Palaeoecol. 132, 97–118.

Stüeken, E.E., Foriel, J., Buick, R., Schoepfer, S.D., 2015. Selenium isotope ratios, redox changes and biological productivity across the end-Permian mass extinction. Chem. Geol. 410, 28–39.

Sun, Y., Joachimski, M.M., Wignall, P.B., Yan, C., Chen, Y., Jiang, H., Wang, L., Lai, X., 2012. Lethally hot temperatures during the Early Triassic Greenhouse. Science 338, 366–370.

Surlyk, F., 1990. Timing, style and sedimentary evolution of Late Palaeozoic-Mesozoic extensional basins of East Greenland. Geol. Soc. Lond. Spec. Publ. 55, 107–125.

Twitchett, R.J., Looy, C.V., Morante, R., Visscher, H., Wignall, P.B., 2001. Rapid and synchronous collapse of marine and terrestrial ecosystems during the end-Permian biotic crisis. Geology 29, 351–354.

Wang, X., Auler, A.S., Edwards, R.L., Cheng, H., Ito, E., Wang, Y., Kong, X., Solheid, M., 2007. Millennial-scale precipitation changes in southern Brazil over the past 90,000 years. Geophys. Res. Lett. 34.

Wignall, P.B., Twitchett, R.J., 1996. Ocean anoxia and the end-Permian mass extinction. Science 272, 1155–1158.

Wignall, P.B., Twitchett, R.J., 2002. Permian–Triassic sedimentology of Jameson Land, East Greenland: incised submarine channels in an anoxic basin. J. Geol. Soc. Lond. 159, 691–703.

Wignall, P.B., Morante, R., Newton, R., 1998. The Permo-Triassic transition in Spitsbergen: $\delta^{13}C_{org}$ chemostratigraphy, Fe and S geochemistry, facies, fauna and trace fossils. Geol. Mag. 135, 47–62.

Wilkin, R.T., Arthur, M.A., 2001. Variations in pyrite texture, sulfur isotope composition, and iron systematics in the Black Sea: evidence for late Pleistocene to Holocene excursions of the O2–H2S redox transition. Geochim. Cosmochim. Acta 65, 1399–1416.

Wilkin, R.T., Barnes, H.L., Brantley, S.L., 1996. The size distribution of framboidal pyrite in modern sediments: an indicator of redox conditions. Geochim. Cosmochim. Acta 60, 3897–3912.

Xiang, L., Schoepfer, S.D., Zhang, H., Yuan, D.-x., Cao, C.-g., Zheng, Q.-F., Henderson, C.M., Shen, S.-z., 2016. Oceanic redox evolution across the end-Permian mass extinction at Shangsi, South China. Palaeogeogr. Palaeoclimatol. Palaeoecol. 448, 59–71.

Xu, D., Lu, H., Chu, G., Wu, N., 2014. 500-year climate cycles stacking of recent centennial warming documented in an East Asian pollen record. Geoscience and Remote Sensing Symposium (IGARSS). 2016 IEEE International.

Yin, H., Sweet, W.C., Glenister, B.F., Kotlyar, G., Kozur, H., Newell, N.D., Sheng, J., Yang, Z., Zakharov, Y.D., 1996. Recommendation of the Meishan section as Global Stratotype Section and Point for basal boundary of Triassic System. Newsl. Stratigr. 34, 81–108.

Zanchettin, D., Rubino, A., Matei, D., Bothe, O., Jungclaus, H.H., 2013. Multidecadal-to-centennial SST variability in the MPI-ESM simulation ensemble for the last millennium. Clim. Dyn. 5, 1301–1318.